LUMA-GIS Thesis nr 15

Exploring the relationship between land surface temperature and vegetation abundance for urban heat island mitigation in Seville, Spain

Andrew Farina

2012

Department of Earth and Ecosystem Sciences

Division of Physical Geography and Ecosystem Analysis

Centre for Geographical Information Systems

Lund University
Sölvegatan 12

A Master thesis presented to

Department of Physical Geography and Ecosystem Analysis

Centre for Geographical Information Systems

of

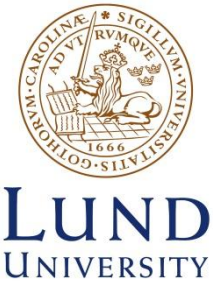

LUND
UNIVERSITY

by

Andrew Farina

in partial fulfilment of the requirements

for the degree of Master in Geographical Information Science

Supervisor:

Ulrik Mårtensson, Lund University

2012

ABSTRACT

The environmental and social consequences of predicted climate change are expected to be amplified in urban environments due to their elevated temperatures, which are attributable to a phenomenon known as the Urban Heat Island (UHI). As vegetation can provide for cooler microclimates through the process of evapotranspiration, increasing amounts of urban vegetation might prove to be a highly effective solution for reducing UHI intensity, thereby mitigating some of the worst effects of predicted climate change. Land Surface Temperatures (LSTs) are considered to be a reliable indicator of the UHI as there is generally a close correlation between LSTs and near-surface air temperatures. Moreover, the Normalized Difference Vegetation Index (NDVI) is widely recognized as a reliable indicator of vegetation abundance. This thesis employed remote sensing and geographic information systems to explore the interactions between LST and NDVI based on land-use/land-cover (LULC) type in Seville, Spain. The findings showed that within the city of Seville, LST and NDVI shared an inverse relationship, implying that an increase in vegetation abundance would generally reduce surface temperatures, and thus UHI intensity. However, this relationship demonstrated that there are distinct differences depending on LULC type. This indicates that increasing the amount of vegetation, with the goal of decreasing UHI intensity, is more effective within certain LULC types than in others. This study therefore illuminated which types of actions would be most conducive to mitigating Seville's UHI.

Keywords: Urban Heat Island, Land Surface Temperature, Normalized Difference Vegetation Index, Land-Use/ Land-Cover, Climate Change

Acknowledgements

I would like to thank my supervisor, Mr. Ulrik Mårtensson, for all his constructive comments and suggestions. My thanks to the European Environment Agency and United States Geological Survey for allowing access to their data. I would also like to extend my deepest gratitude to my family for their constant moral support and love.

Contents

List of Abbreviated Terms

BLHI	Boundary Layer Heat Island
BSh	Semi-Arid Climate
CLHI	Canopy Layer Heat Island
CO_2	Carbon Dioxide
Csa	Mediterranean Climate
DN	Digital Number
EEA	European Environment Agency
ETM+	Enhanced Thematic Mapper Plus
FCC	False Color Composite
GIS	Geographic Information Systems
GMES	Global Monitoring for Environment and Security
LST	Land Surface Temperature
LSE	Land Surface Emissivity
LULC	Land-use/ Land-cover
NDVI	Normalized Difference Vegetation Index
SUHI	Surface Urban Heat Island
TM	Thematic Mapper
UHI	Urban Heat Island
USGS	United States Geological Survey
UTM	Universal Transverse Mercator

1. Introduction

1.1 Background

The current rate of global urbanization is accelerating dramatically, with nearly 70% of the world's human population projected to be living in urban areas by 2050 (UN, 2007). At the same time we have climate changes which are expected to be present for at least 30 to 40 years into the future, due in part to the long shelf-life of carbon dioxide (Hulme et al., 2002). Moreover, the effects of climate change are expected to be amplified in urban areas due to their distinctive biophysical features (Gill et al., 2007; Fortuniak, 2009). Therefore, regardless of whether greenhouse gas emissions will be reduced in the future, climate change is here to stay and thus, there is a need to develop adaptive strategies to prepare the world's expanding urban centers in an attempt to diminish some of its worst effects.

1.1.1 The urban heat island phenomenon

The most significant biophysical feature of the urban environment distinguishing it from surrounding rural areas is its altered surface cover, a contributor to the phenomenon commonly referred to as the Urban Heat Island (UHI) (Gill et al., 2007). The UHI phenomenon describes the excess warmth of the urban environment as compared to its rural surroundings. This heat discrepancy is due to differences in the relative surface cooling rates between urban and rural areas (Voogt, 2002; Weng et al., 2004). Thus, the term 'urban heat island' has been designated to describe the relative elevated temperatures found over urban areas (Voogt, 2002), appearing as an "island" in the pattern of isotherms on a map (Geer, 1996).

Atmospheric and surface temperatures within urban environments are generally warmer than their peripheries. This is due to the replacement of natural green surfaces with non-evaporative and non-porous urban materials with high heat capacity and low solar reflectivity, such as concrete masses, asphalt roads and metal surfaces. These materials exhibit a high degree of thermal inertia (Arrau and Pena, 2010) and are characterized by a high level of absorption of solar radiation, with a greater capacity for thermal conductivity as compared to natural surfaces (Rose and Devadas, 2009). Such surface materials cause a reduction in potential cooling rates within urban areas, as compared to their surroundings (Lo et al., 1997). This difference in cooling rates is what produces the UHI. Also, as urbanization tends to result in a decrease in overall vegetation, evaporative cooling is drastically diminished, resulting in urban areas being much warmer than their peripheries (Lo et al., 1997; Rose and Devadas, 2009).

1.1.1.1 Spatial characteristics of the UHI

The spatial characteristics of the UHI are contingent upon the configuration and topographic setting of the urban area, however, the spatial pattern of UHI isotherms are typically aligned with the urban-rural boundary (Voogt, 2002). Moreover, the increased temperatures associated with the UHI phenomenon are not uniform across the urban area as a whole, as

intra-urban thermal patterns are generally influenced by urban surface features (Santana, 2007). A sketch of a typical UHI profile is provided in Figure 1, (note how atmospheric temperatures vary over different surface features).

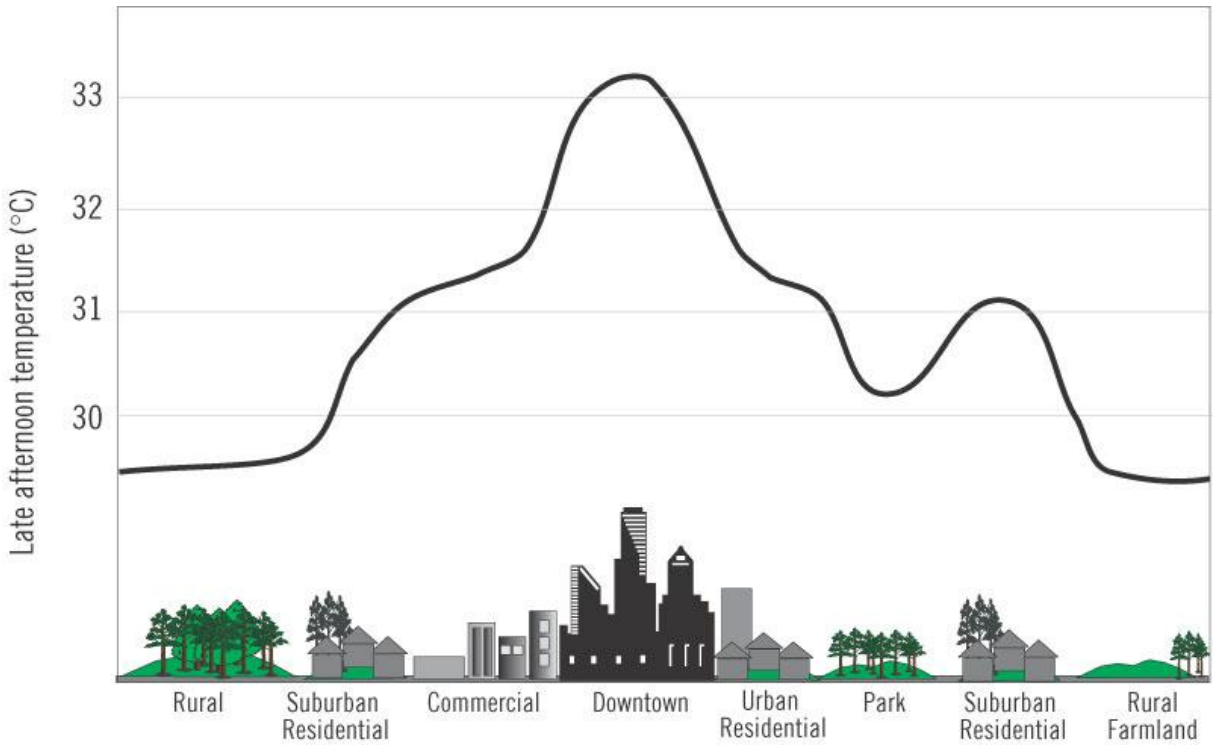

Figure 1. *Sketch of a typical UHI profile. Source: Arrau and Pena, 2010.*

1.1.1.2 UHI intensity

UHI's are usually most pronounced during the nighttime as the majority of urban materials tend to absorb heat during the day which is then only slowly released during the nighttime hours (see Figure 2). This is due to their high thermal inertia. By the time most rural surfaces have already experienced cooling after sunset; most urban materials will have only partially cooled, releasing heat at a much slower rate (Arrau and Pena, 2010). The result is a modified urban climate, much warmer than its non-urbanized surroundings (Rose and Devadas, 2009). Moreover, the differential cooling rates between urban areas and their rural peripheries are usually most distinct on calm and clear nights. It has been found that cities with populations of 1 million or more average 1 to 3°C warmer in atmospheric temperature as compared to their rural surroundings (EPA, 2009a). However, in some cases this temperature discrepancy has been measured to be as much as a 12°C difference (University of Manchester, 2007).

The magnitude of an UHI is known as UHI intensity, which can be defined as the air temperature difference between urban and rural areas. UHI intensity is influenced by climate region, local topography, industrial development of a city (Stathopoulou et al., 2005) city size and density, Land-Use/Land-Cover (LULC) characteristics, the characteristics of the surrounding rural areas (Fortuniak, 2009) and vegetation abundance (Santana, 2007). Meteorological conditions (especially wind speed and cloud cover) and sun intensity also influence the development of the UHI – and therefore, UHI intensity tends to vary both hourly

and seasonally (EPA, 2009a). Of all the factors mentioned above, LULC characteristics and the abundance of urban vegetation are the two factors which are considered to have the most significant effect on UHI intensity, as well as on intra-urban thermal patterns (Xian and Crane, 2006; Arrau and Pena, 2010).

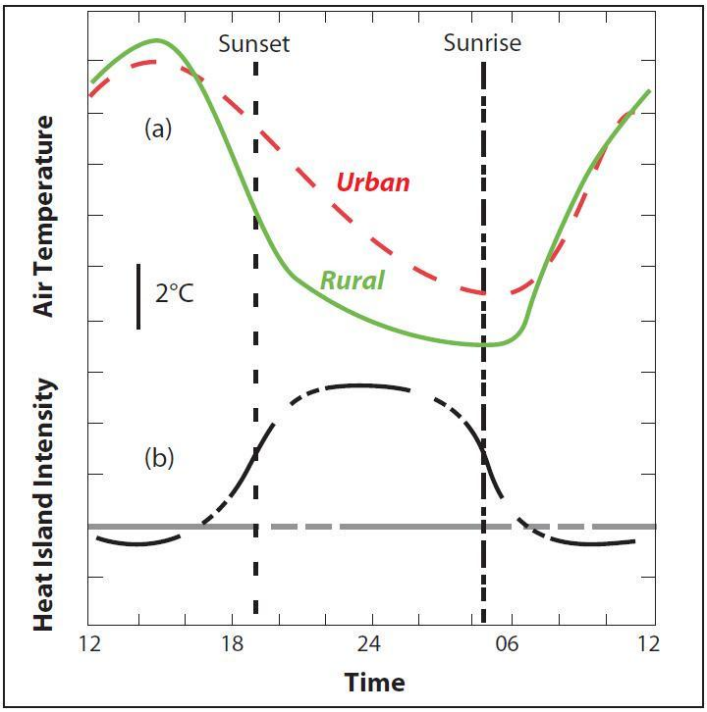

Figure 2. *Conceptual drawing of the development of the UHI under conditions of clear skies and a weak airflow. Section (a) denotes the typical differential cooling rates between urban and rural areas. Section (b) denotes the typical diurnal evolution of UHI intensity. Source: modified from EPA, 2009a.*

1.1.2 Types of UHIs

1.1.2.1 Atmospheric urban heat islands

Atmospheric urban heat islands can be divided into two different categories: Canopy Layer Heat Island (CLHI) and Boundary Layer Heat Island (BLHI). The CLHI refers to the layer of air closest to the surface which extends to approximately building height. The BLHI is located above the canopy layer and may be up to 1 kilometer or more in thickness by day and a few hundred meters in thickness at night (Voogt, 2004). Of the two types of atmospheric heat islands, CLHIs are the ones most commonly observed and referred to in the majority of UHI research. Therefore, this study will use the term urban heat islands (or UHIs) to refer to CLHIs.

1.1.2.2 Surface urban heat island

The Surface Urban Heat Island (SUHI) refers to the relative warmth of urban surfaces compared to surrounding non-urbanized surfaces. While the atmospheric UHI can be detected

by ground-based air temperature measurements, the SUHI is typically characterized as a measurement of Land Surface Temperature (LST), based on the use of thermal remote sensing (Rose and Devadas, 2009). SUHIs are generally strongest during the day but are usually present during the night as well. Similar to UHIs, the magnitude of SUHIs is influenced by sun intensity, LULC characteristics and vegetation abundance. SUHIs are typically largest during the summer and their intensity tends to vary much more than that of UHIs (EPA, 2009a). The difference in daytime surface temperatures between urban and rural areas is on average 10 to 15°C, however, at night the difference in surface temperatures between the two tends to average only about 5 to 10°C (Voogt and Oke, 2003).

1.1.2.3 Relationship between surface and air temperatures

LSTs are considered to be a reliable indicator of the UHI as there is generally a high correlation between LSTs and air temperatures in the canopy layer, due to the transfer of thermal energy emitted from the surface to the atmosphere (Nichol, 1994; Arrau and Pena, 2010). However, due to the fact that air mixes within the atmosphere, the relationship between surface and near-surface air temperatures is not constant (EPA, 2009a). As can be observed in Figure 3, atmospheric temperatures normally fluctuate less than surface temperatures across a given area during the day, while a more congruent relationship between atmospheric and surface temperatures can be observed during the nighttime hours.

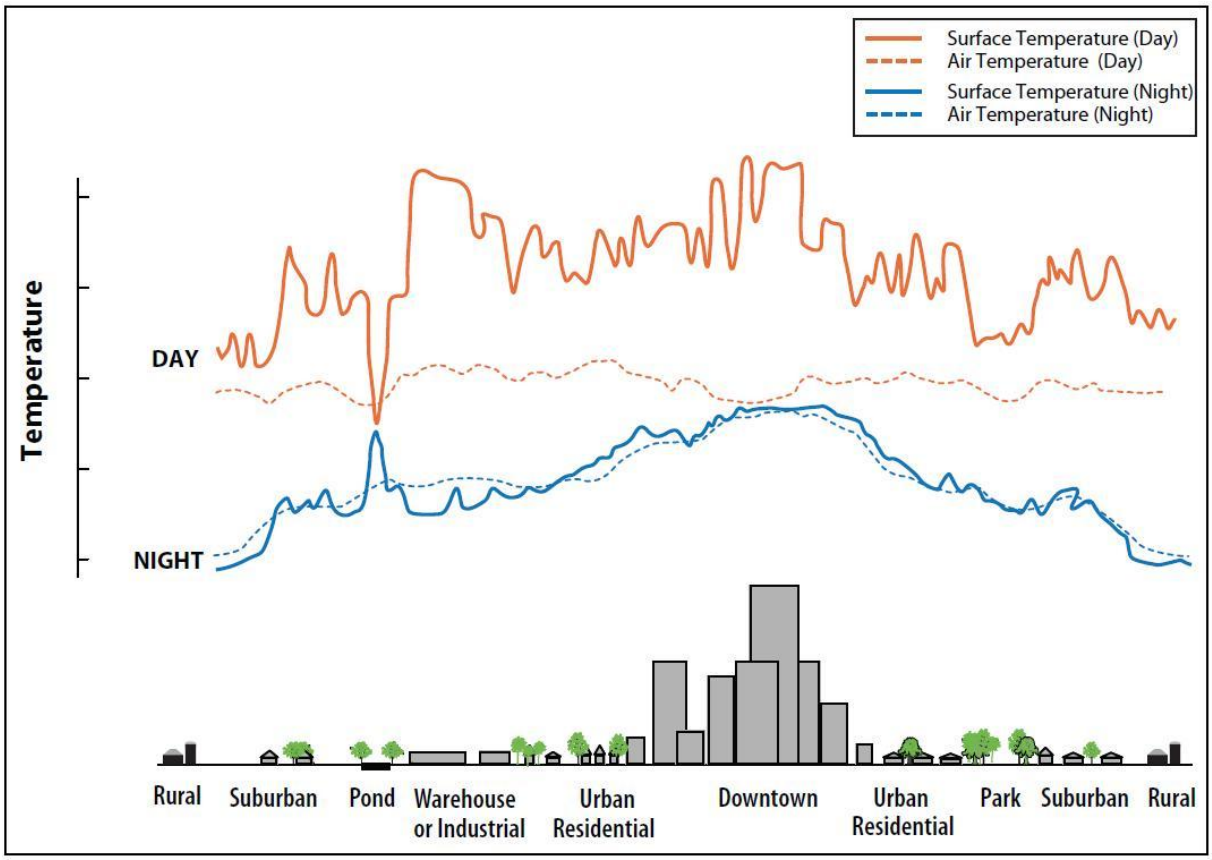

Figure 3. *Variations in Atmospheric and Surface temperatures. Source: EPA, 2009a.*

1.1.3 Environmental and social impacts

Although there may be certain positive impacts attributable to the increased temperatures associated with UHIs (including the melting of ice on roads during the winter, reductions in energy required for heating, and longer plant-growing season), such potential benefits are largely outweighed by the substantial detrimental environmental and social aspects discussed below (EPA, 2009a).

1.1.3.1 Environmental impacts

1.1.3.1.1 Increased energy consumption and greenhouse gasses

The increased temperatures associated with the UHI are known to have major negative environmental impacts, not only on urban environments but also on ecosystems in rural areas (Arrau and Pena, 2010). In fact, UHIs can contribute, in an indirect manner, to climate change as elevated summertime temperatures in cities often result in the need for increased energy consumption due to a higher demand for air conditioning. This, in turn, often requires increased use of fossil-fuel powered plants, increasing emissions of greenhouse gases such as Carbon Dioxide (CO_2) into the atmosphere (Santana, 2007; EPA, 2009b). Urban electricity demands are known to rise on average 1.5 to 2% for every 0.6°C increase in air temperatures, starting from about 20 to 25°C (EPA, 2009b). One study showed that, within the United States, 5-10% of urban peak electricity demand is used to compensate for the UHI effect (Akbari, 2005). Figure 4 demonstrates how electrical loads for the city of New Orleans steadily increase once temperatures exceed about 20 to 25°C.

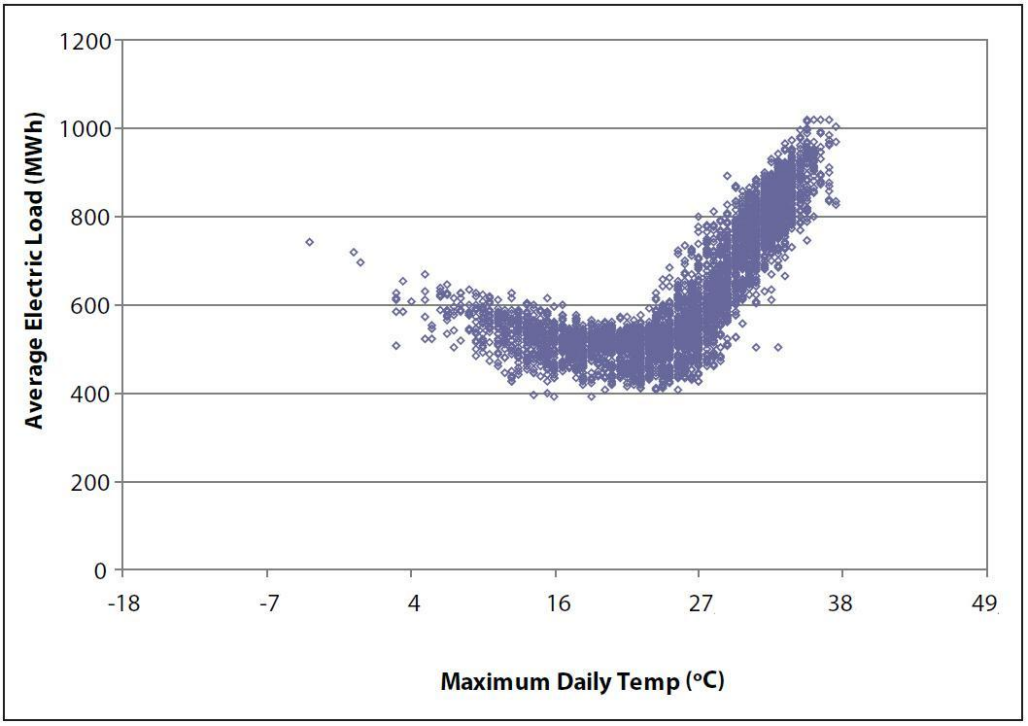

Figure 4. *Electricity used per hour in relation to outdoor temperature (New Orleans). Source: modified from EPA, 2009a.*

1.1.3.1.2 Air quality

In addition to greenhouse gas emissions, the increase in energy demand associated with elevated summer temperatures also often results in higher levels of air pollution as fossil-fuel powered plants (which currently provide about 66% of global electricity) emit Nitrogen Oxides (NO_x), Mercury (Hg), Carbon Monoxide (CO), Sulfur Dioxide (SO_2), and Particulate Matter (PM) into the atmosphere (EPA, 2009a; WWF, 2010). These pollutants are known to have a detrimental effect on air quality, contributing to acid rain and other phenomena which may be damaging to human health. Higher urban temperatures are also known to increase ground-level ozone (see Figure 5), which is the result of a reaction between Organic Compounds *(VOCs)* and NO_x (Santana, 2007; EPA, 2009a).

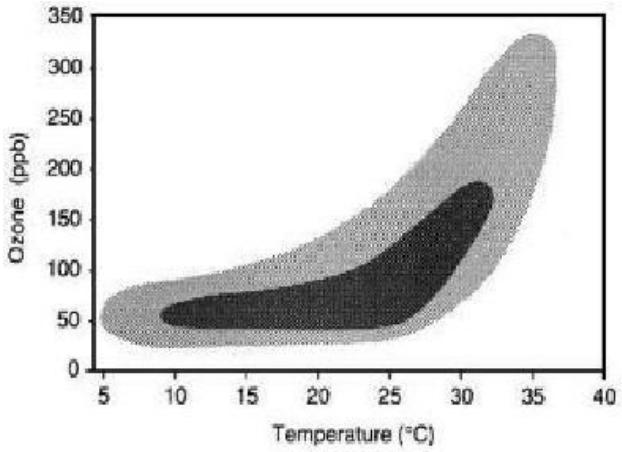

Figure 5. *Relationship between daily maximum ozone concentration and daily maximum atmospheric temperatures in Connecticut. Shading is based upon density of data points. Source: Oke, 1997.*

1.1.3.1.3 Increased instability of the urban atmosphere

The UHI phenomenon is known to reduce the stability of the urban atmosphere at night which, under certain meteorological conditions, may intensify the proliferation of convective clouds. Thus, the effect of rainfall events (which according to the Intergovernmental Panel on Climate Change are expected to increase in magnitude and frequency due to climate change) may be amplified in urban areas, resulting in economic losses and extra costs due to, among other things, the need for improvements in storm-water drainage (Parry et al. 2007; Fortuniak, 2009).

1.1.3.2 Social impacts

1.1.3.2.1 Human health

Since UHIs tend to exacerbate the impact of heat waves, heat-related fatalities are another consequence of increased urban temperatures (see Figure 6) (EPA, 2009a). For example, the 2003 heat wave over Europe caused an estimated 35,000 fatalities (Gill et al., 2007). Due to the UHI, temperatures during heat waves often do not cool off significantly during the night.

High nighttime temperatures during heat waves are associated with increased mortality even more so than high daytime temperatures since there is no break from the heat, giving people no significant relief (Kalkstein, 1991). In addition to heat-related mortality, increased urban temperatures may also contribute to heat cramps, exhaustion, non-fatal heat stroke and general discomfort (EPA, 2009a). Climate change is expected to intensify such impacts, as current climate change models predict a general increase in summer temperatures and longer durations of heat waves (Gill et al., 2007).

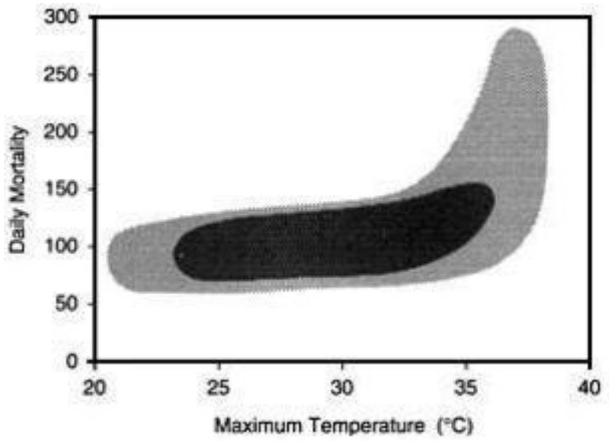

Figure 6. *Relationship between mortality and maximum atmospheric temperature in Shanghai (1980 to 1989). Note that at temperatures above 34 ºC there is a marked increase in heat-related deaths. Shading is based upon density of data points. Source: Oke, 1997; data adapted from the original research by Kalkstein and Smoyer, 1993.*

1.1.4 UHI mitigation through increased urban vegetation

1.1.4.1 The cooling effect of vegetation

The abundance of urban vegetation is known to greatly influence the urban thermal environment and the development of the UHI. Vegetation can reduce LSTs and atmospheric temperatures through evapotranspiration (Yuan and Bauer, 2007; Ramachandra and Kumar, 2010), a process by which heat from the air results in the evaporation of water (EPA, 2009c). Evapotranspiration is believed to be able to cause a reduction in peak summer temperatures within urban environments by as much as 1 – 5°C (EPA, 2009b).

1.1.4.1.1 Evapotranspiration

In general, evapotranspiration is the combined process of evaporation and transpiration. Evaporation refers to the loss of water to the atmosphere from soil and plant surfaces, whereas transpiration refers to the loss of water to the atmosphere from plant tissues (CIMIS, 2009). While plants are still small in size water is mostly lost through soil evaporation, however, once plants grow larger and begin to cover the soil water will mostly be lost to the atmosphere through transpiration (FAO, 1998). Transpiration rates vary widely and are determined by a number of factors including temperature, relative humidity, wind and air movement, soil-moisture availability and plant species (USGS, 2010a).

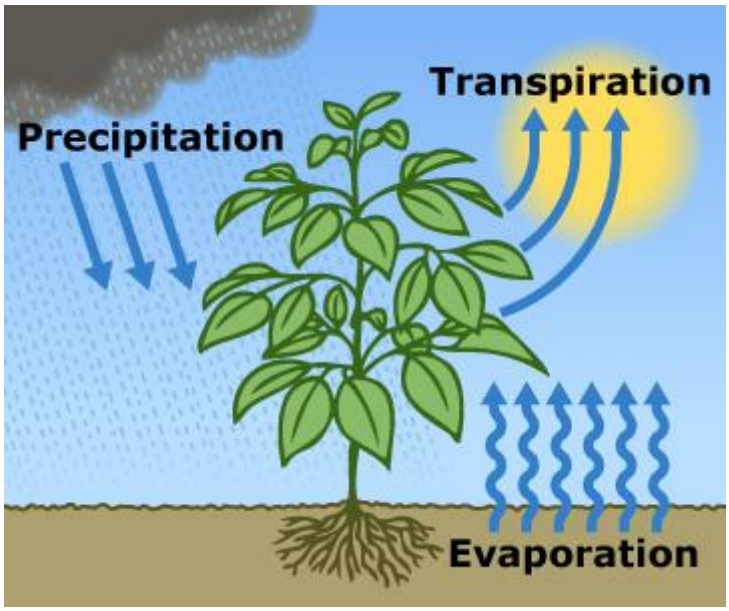

Figure 7. *Evapotranspiration is the sum of plant transpiration and evaporation from plant surfaces and surrounding soil. Source: WateReuse Foundation, 2007.*

1.1.4.2 Benefits and costs

Increasing vegetative cover is widely recognized as a simple and effective way to reduce UHIs and make urban environments less vulnerable to some of the worst effects of climate change (EPA, 2009b; Fortuniak, 2009). A number of initiatives have, therefore, appeared in recent times promoting greater awareness of the functionality provided by urban vegetation (The City Arborist Program, 2001; Arbor Day Foundation, 2010; Tree Utah, 2010). A series of studies have also been published investigating the relationship between the urban thermal environment and vegetation abundance, as well as the benefits of increasing vegetative cover in urban areas (Weng et al., 2004; Amiri et al., 2009; Huang et al., 2009). For example, a recent study revealed that a 10% increase in the amount of vegetation in Manchester could possibly reduce temperatures in this urban environment by as much as 4°C, potentially offsetting urban temperature increases over the next 75 years, in relation to the current climate change models (University of Manchester, 2007).

Another significant benefit of the cooler urban temperatures provided by urban vegetation, in relation to climate change, is the reduction of overall energy consumption used for air-conditioning which, in turn, decreases emissions of greenhouse gasses and associated air pollution (Yue et al., 2007). Moreover, one study found that the extensive implementation of UHI mitigation measures, including increasing urban vegetation, could reduce air-conditioning demand in the United States by an estimated 20%, which would amount to a savings 40 terawatt-hours per year (Akbari, 2005). Urban vegetation can also help to remove gaseous pollutants produced within city centers and offset city-wide CO_2 emissions (McPherson et al., 2005).

Other benefits of urban vegetation include aesthetic enhancement and the psychological benefits experienced by urban residents in the form of increased overall well-being and

quality of life (Yue et al., 2007). In addition, urban vegetation may also help lessen storm-water runoff and enhance water quality by filtering precipitation (EPA, 2009b). Using urban vegetation as a means to mitigate the UHI may also help reduce the negative social impacts of increased summertime temperatures and the longer duration of heat-waves associated with climate change (Gill et al., 2007; EPA, 2009a). Likewise, such mitigation measures might also help to stabilize the urban atmosphere, potentially reducing the possible negative impacts of rainfall events, which, as mentioned above, are predicted to increase in magnitude and frequency as a result of climate change (Parry et al., 2007; Fortuniak, 2009).

The main costs associated with planting vegetation in urban areas include the purchase of materials, planting and maintenance activities. However, the benefits of increasing urban vegetation, such as energy savings, air quality improvement and storm-water retention, are considered to almost always outweigh associated costs (EPA, 2009c). For instance, a five-city study conducted in the United States revealed that, on a per-tree basis, for every dollar invested, cities accrued benefits estimated to range from about $1.50 to $3.00 (McPherson et al., 2005).

1.1.5 Measuring the urban thermal environment and vegetation abundance

There are a variety of approaches to the measurement of the urban thermal environment including mobile sampling of air and surface kinetic temperatures from ground and airborne vehicles, sampling of air and surface kinetic temperatures at fixed locations, and the remote measurement of LSTs from space-borne platforms. However, remote sensing is considered to be one of the most useful tools for detecting thermal variations within urban settings due to the ability of this tool to collect scores of spatially contiguous samples over large areas instantaneously (Yue et al., 2007). Moreover, the remote sensing method can provide measurements regarding the spatial extent of surface heat island effects for metropolitan areas as well as regarding the magnitude of surface temperatures (Yuan and Bauer, 2007). Remote sensing is also a valuable tool to use in studying urban vegetation as it can obtain data which can be used to quantify the extent and condition of vegetation (Yue et al., 2007).

Although the application of remote sensing in studies related to the urban environment has been rather limited due to sensor resolutions which are often too coarse for the identification of individual structures, the Landsat 7 Enhanced Thematic Mapper Plus (ETM+) sensor has resolutions which can be considered sufficient for detecting significant spatial variations in surface temperature as well as in urban vegetation (Yue et al., 2007).

1.1.6 The normalized difference vegetation index

The Normalized Difference Vegetation Index (NDVI) is a vegetative index used in remote sensing analysis to assess whether or not a target contains live green vegetation. Healthy vegetation is highly absorbent of visible light (0.4 to 0.7 μm) and reflects most near-infrared light (0.7 to 1.1 μm). Unhealthy or sparse vegetation, on the other hand, will generally reflect more visible light and less near-infrared light (FSNAU, 2010). Therefore, greater reflected radiation in the near-infrared wavelengths than in the visible wavelengths generally indicates the presence of green vegetation, whereas little difference in the intensity between the two

wavelengths is generally an indicator of sparse vegetation or non-vegetated surfaces (Weirer and Herring, 2010). As the near-infrared and red bands of satellites are those most sensitive to vegetation information, these bands can be employed to quantify the density of plant growth in a given pixel (FSNAU, 2010; Weirer and Herring, 2010).

NDVI values will typically range between -1 and 1 where the higher the value, the healthier and denser the vegetation. Moreover, values greater than 0.2 usually indicate vegetation, whereas values below 0.2 generally indicate soil, rock, or man-made materials. Water bodies typically give negative NDVI values (Liao et al., 2005; Tam et al., 2010).

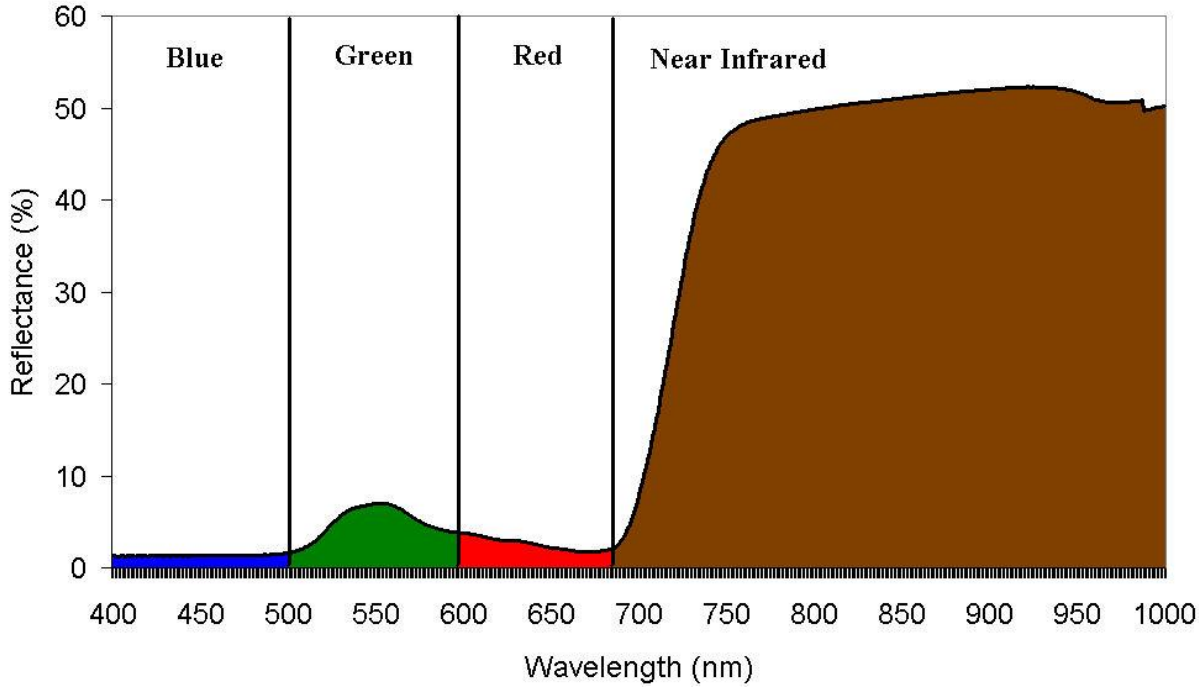

Figure 8. *The spectral curve of vegetation. Source: SEOS, 2010.*

1.1.6.1 The relationship between NDVI and LST

As stated above, LSTs correspond closely with near surface temperatures and can therefore be considered a reliable indicator of the UHI. Vegetation abundance is also known to influence LSTs and UHI conditions through the process of evapotranspiration. Therefore, investigation into the relationship between NDVI and LST becomes informative and meaningful, especially in regards to areas where the UHI phenomenon is more pronounced and where mitigation measures are needed.

Given that vegetation abundance is known to reduce LSTs through the transfer of latent heat from the surface to atmosphere via evapotranspiration, NDVI can be used to investigate this relationship and thereby, provide insight into how this natural cooling mechanism of vegetation might be employed to help improve urban thermal environments. In general, areas with high NDVI will typically have lower LSTs, however, this correlation may be influenced by soil moisture conditions and evapotranspiration of the surface (Yuan and Bauer, 2007; Su et al., 2010).

1.1.7 LULC and the urban thermal environment

LULC characteristics are known to have a significant influence on intra-urban thermal conditions (Xian and Crane, 2006). For example, Roth et al. (2008) found a strong correlation between LULC and intra-urban thermal patterns with industrial areas being the warmest and vegetated, riverine and coastal areas being the coolest. As different LULC characteristics can modify thermal conditions in cities, an enhanced understanding of the interrelationship between LULC and LST can be employed in order to improve urban planning decisions aimed at UHI mitigation (Santana, 2007).

1.2 Objective

As previously stated, the main reasons for the UHI phenomenon include urban materials of high heat capacity and low solar reflectivity such as concrete and asphalt and reduced evaporative cooling due to the replacement of natural green surfaces with impervious surfaces. Intra-urban thermal patterns are known to be strongly linked to LULC characteristics and vegetation abundance with vegetated surfaces capable of decreasing UHI intensity as they provide for cooler microclimates.

In a world facing rapid urbanization (which often leads to a reduction in green areas) as well as a changing climate, it becomes increasingly important to understand the influence which LULC and vegetation have on the urban thermal environment. Such knowledge can be applied to urban design strategies in which urban vegetation is used as a means to reduce UHI intensity and moderate the increase in urban summer temperatures anticipated to occur with climate change.

The main objective of this study is to analyze the interactions between LST and NDVI based on LULC using the city of Seville, Spain as a case study. The aim of the research is to contribute to the understanding of the manner by which vegetation components of the urban ecosystem impact the urban thermal environment. It is the objective of this study that the findings and correlations regarding the influence of LULC and vegetation on LST could serve to be useful for urban planning and management strategies focused on UHI mitigation and the adaptation of cities to the challenges of climate change. Moreover, it will address the following research questions:

1. What is the general relationship between LST and NDVI in the study area?

2. What is the relationship between LST and NDVI for each LULC type?

3. Which LULC types might be most conducive to reducing urban temperatures through an increase in vegetation?

4. Which residential LULC types might be most conducive to reducing urban temperatures through an increase in vegetation?

2. Study Area

The city of Seville (37°21′55″N, 6°0′30″W) is located in the southwest of the Iberian Peninsula and is the capital of the Autonomous Community of Andalusia (Consorcio de Turismo, 2003; AEMET, 2010). The city has a surface area of about 73 km^2 (Fuentes and Rowe, 1998) and as of 2010, the population within the Seville urban area was comprised of 704,198 inhabitants, making it the fourth largest city in Spain (INE, 2010). It is situated in the Guadalquivir valley along the banks of the Guadalquivir River and has an average elevation of 6 meters above sea level. Although the city of Seville is surrounded by numerous satellite towns (Consorcio de Turismo, 2003), the study area (depicted in Figure 9) was limited to the urban core of Seville for reasons which will be covered in Chapter 3.

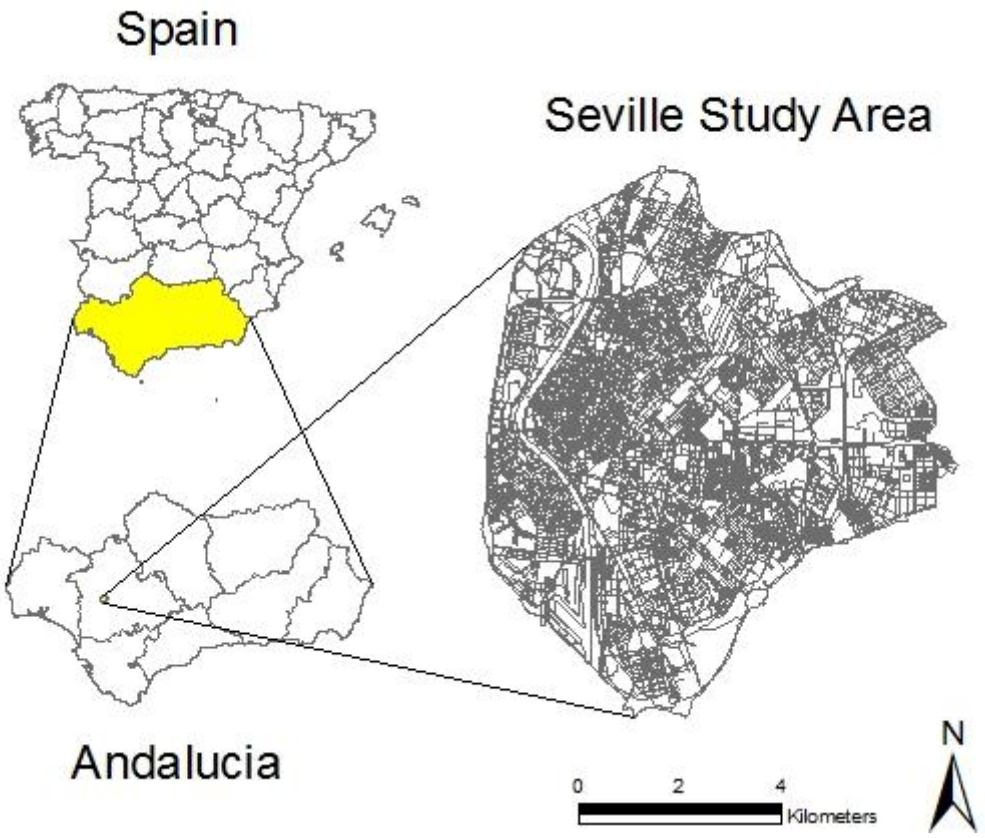

Figure 9. *Map showing the study area. Source: adapted from GADM, 2009; adapted from EEA, 2010a.*

2.1 Climate

According to Köppen's climate classification system, Seville has a Mediterranean Climate (Csa) with Semi-Arid Climate (BSh) influences (see Table 1a and b for description of Csa and BSh climates) (Climate, 2007; Sevilla Weather, 2009). Seville experiences mild winters and blazing hot summers (Sevilla Weather, 2009) and is considered to be one of the warmest cities in Europe (AEMET, 2007). July is its warmest month with average maximum temperatures of 35.5°C and average minimum temperatures of 18.9°C (AEMET, 2010) and

every summer temperatures typically exceed 40°C on several occasions (Sevilla Weather, 2009). January is the coolest month in Seville with average maximum temperatures of 16°C and average minimum temperatures of 5.7°C (AEMET, 2010). Average air temperatures in Seville for each month of the year are displayed in Figure 10. Since Seville is located about 60 kilometers away from the Atlantic Ocean, temperatures are sometimes modified by mild sea breezes (Sevilla Weather, 2009). Seville receives an average total rainfall of 554 millimeters per annum, which is concentrated within the period of October to April. The average annual relative humidity of Seville is about 70% (AEMET, 2010).

Table 1a. *Köppen's definition of Mediterranean Climate (Csa). Source: Climate, 2007.*

Symbol	Description
C	Hot moderate climate. The three coldest months average a temperature between -3°C and 18°C. Warmest month average temperature > 10°C. The summer and winter seasons are well defined.
s	Dry season in summer.
a	Hot summer. Average temperature of the warmest month > 22°C.

Table 1b. *Köppen's definition of Semi-Arid Climate (BSh). Source: Climate, 2007.*

Symbol	Description
B	Dry climate/desert. Annual evaporation higher than precipitation. No permanent rivers.
S	Steppe climate (semi-arid). Annual precipitations range between 380 and 760 mm.
h	Dry and heat. Annual average temperature > 18°C.

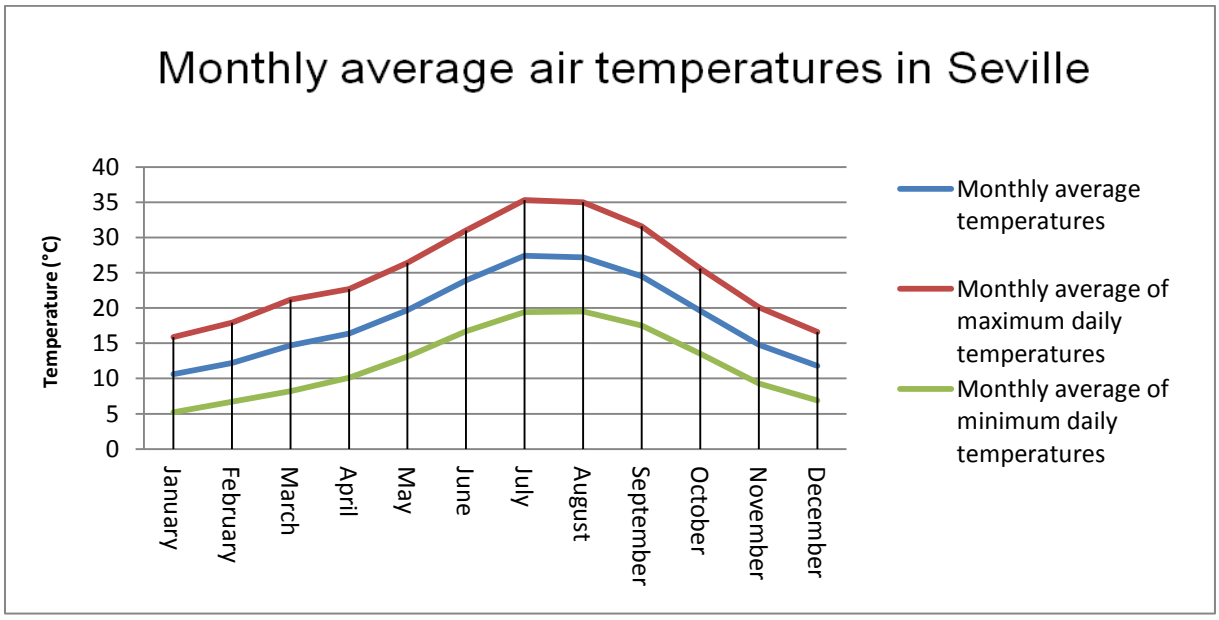

Figure 10. *Temperature diagram showing monthly average temperatures, monthly average of maximum daily temperatures, and monthly average of minimum daily temperatures for Seville. Based on 29 years of data (1971-2000). Source: adapted from AEMET, 2010a.*

2.2 Recent urban development

Over the past twenty years, Seville has seen major investments in its infrastructure as well as massive growth in its industrial activities. Today the city has a highly diversified industrial sector with major growth potential and contains a large number of newly developed industrial and commercial parks and technology centers. Seville is considered to be the strongest economically of all the cities in Andalusia as its newly expanded infrastructure continues to foster the growth of its economy, which is primarily dominated by the service sector and industry. In fact, Seville's recent production and job growth rates have been higher than the Spanish and European Union averages (Sevilla Global, 2010). During the past 20 years, Seville's urban area has experienced a substantial growth in population and the city constitutes the center of an expanding metropolitan area (Gay and Valverde, 2010).

2.3 Seville as a study area

There are a number of reasons why Seville is an ideal area for studying the environmental influences of urban LULC and the relationship between the urban thermal environment and vegetation abundance. Seville has notoriously high summer temperatures which make the urban area prone to heat islands of great intensity. The city also often experiences high humidity and low wind speeds (AEMET, 2010) and when such conditions coincide with high temperatures, the frequency of fatalities due to heat stress increases dramatically (Kalkstein, 1991). The fact that Seville is a location where increased temperatures may have such a dramatic impact emphasizes the importance of understanding the consequences of planning decisions and the issue of reducing risk through improved urban planning.

As mentioned above, Seville has experienced considerable growth in its industrial activities in recent times. Industrial activities continue to be established within the Seville area, including those areas included in the study area. The manner in which new industrial areas are developed will undoubtedly have an effect on Seville's urban thermal environment. Thus, the analysis will attempt to provide the basis for decision making regarding urban and ecological planning in Seville. In other words, through the examination of the effects of existing development, the aim is that planners will be able to use such information to shape policies which may reduce the negative environmental impacts of future industrial expansion.

In addition to its industrial expansion, it is likely that the city will also experience continued expansion of its residential areas in the near future as the city has recently experienced a substantial growth in population (Gay and Valverde, 2010) and remains a main growth center in Spain (Encyclopedia of the Nations, 2010). Therefore, the study will also attempt to provide insight into the impact which various types of residential LULC types might have on Seville's thermal environment in order to promote improved planning of residential areas. Another reason why Seville is an ideal area for the evaluation of environmental impacts of urban LULC zoning has to do with its diversity of LULC types and the fact that the city contains many urban gardens (Andalucia Com SLU, 2010), thereby lending more credibility to results and analysis regarding the impact of vegetation components on urban thermal environments.

3. Data and Methods

This chapter describes the data used in the analysis and outlines all data pre-processing, preparation and processing methods performed in the study. ESRI ArcGIS^{TM} software was employed to complete all the procedures summarized in this chapter. A flowchart of all GIS (Geographic Information Systems) functions executed in the study is provided in Appendix I.

3.1. Data

3.1.1 Satellite imagery

A Landsat 7 ETM+ image acquired on May 18th 2003 was used to derive LST and NDVI over the study area. The image, which was acquired from the United States Geological Survey (USGS), was captured at approximately 12:51 p.m. local time under clear atmospheric conditions (0% cloud coverage).

At the time of image capture the air temperature in Seville was approximately 30°C and the humidity was 35%. The wind speed at this time was approximately 2.1 m/s and was blowing in an easterly direction. The maximum temperature recorded in Seville on May 18th 2003 was 34°C and the minimum temperature recorded was 15°C (Weather Underground, 2010).

It should be noted that when studying the UHI anomaly through contrasts between LSTs, that SUHI intensities are at their greatest during the afternoon, at least during the warm season. This is the opposite of UHI results based on the measurement of air temperatures where the anomaly will typically reach its greatest intensity during the nighttime (Weng et al., 2004). Therefore, the selection of the May 18th image, which was the best image available given that it was captured in the afternoon, is suitable.

The May 18th image was also selected for the reason that it falls within the early part of the warm season when green vegetation is likely to be in abundance. The presence of green vegetation is paramount to a study concerned with the association between LSTs and NDVI, as NDVI is an indicator of biomass production and is therefore impacted by seasonal changes (Yuan and Bauer, 2007). Another reason why this particular image was chosen has to do with the fact that for mid-latitude cities, such as Seville, UHI intensities are often strongest during the warm season (Voogt, 2004). Thus, a study which attempts to establish an understanding of how biological solutions might help alleviate UHI's through the analysis of intra-urban relationships between LST and NDVI (the values of which are likely to vary significantly between seasons), becomes much more meaningful if the data used to derive these variables are captured during a time of year when heat island intensity is most extreme and poses the greatest risk to society and the environment.

A Landsat 5 Thematic Mapper (TM) image acquired on August 9th 2007 at approximately 12:56 p.m. local time under clear atmospheric conditions (0% cloud coverage) was also used in this study. The image, which was acquired from the USGS, was used for the purpose of indentifying areas within the study area where LULC had changed between May of 2003 and August of 2007. This was necessary as the LULC data over Seville used in the analysis were

created through the photo interpretation and vector digitization of four Spot 5 images which were captured on August 22nd, 2007, implying that there was a possibility that the data did not represent actual LULC in Seville as of May 18th 2003. Further explanation as to how the Landsat TM image was used to detect LULC change between May of 2003 and August of 2007 is provided in section 3.2.2 "LULC data pre-processing". It should be noted that the reason why the Landsat TM image acquired on August 9th 2007 was not used for deriving LST and NDVI over the study area was due to the TM sensor's low thermal band spatial resolution of 120 meters, which would not be suitable for detecting the complex temperature differences within the urban area of Seville.

3.1.2 LULC data

As noted in Section 3.1.1, a dataset depicting LULC over the Seville metropolitan area was used for this research. The dataset, which is included as a part of the Global Monitoring for Environment and Security (GMES) Urban Atlas database was acquired from the European Environment Agency (EEA). The GMES Urban Atlas database provides high resolution LULC data in vector format for large urban areas in Europe. The dataset over Seville describes LULC for the metropolitan area using a nomenclature of 20 classes at a scale of 1:10000 (EEA, 2010a).

3.2 Data pre-processing and preparation

3.2.1 Satellite imagery pre-processing

Due to the fact that both the Landsat ETM+ and Landsat TM images were captured under clear conditions (0% cloud coverage for both images), uniform atmospheric conditions within the images were assumed and no atmospheric corrections were applied.

Both images were preprocessed by the USGS in order to rectify any geometric or radiometric distortions of the image to a level of 1G product. This correction process employs both digital elevation models and ground control points to achieve a product that is free from distortions related to the Earth (e.g. curvature, rotation), satellite (e.g. attitude deviations from nominal), and sensor (e.g. view angel effects). The USGS also geometrically corrected and georeferenced both images to the WGS1984 datum and Universal Transverse Mercator (UTM) zone 29N coordinate system (Landsat Project Science Office, 2001; USGS, 2010b).

3.2.2 LULC data preparation

The GMES Urban Atlas dataset over the Seville metropolitan area was first rectified to the WGS1984 datum and UTM zone 29N coordinate system.

Since the intention of the study is to contribute to the understanding of the negative effects of urban development and the ways in which these effects might be mitigated, a decision was made to delimit the study area to the urban core area of Seville and exclude surrounding satellite towns. By restricting the study area to the vicinity wherein UHIs are most likely to develop, one can achieve a better comparative understanding as to which types of urban

LULC are most detrimental to the urban thermal environment. Such results can then be used to modify existing polices which may serve to allow for a reduction in environmental impacts caused by further development.

Various motorways that encircle the urban core of Seville were used to define the boundaries of the study area and the GMES Urban Atlas dataset over the Seville metropolitan area was clipped to include areas only within this perimeter. These motorways included Route SE-30, Route A8028, Route SE-020, Avenue Carlos III, Avenue del Deporte, and Calle Taiwan.

As mentioned in Section 3.1.1, due to the fact that the GMES Urban Atlas dataset for Seville was created through the photo interpretation and vector digitization of satellite images which were acquired on August 22nd 2007 there was a possibility that the LULC depicted in the dataset did not represent actual LULC in Seville as of May 18th 2003. Therefore, a Landsat TM satellite image acquired on August 9th 2007 was employed to identify changes to LULC within the study area between these dates.

In order to identify changes to LULC within the study area, False Color Composites (FCC) were created for the Landsat ETM+ data acquired on May 18th 2003 and the Landsat TM data acquired on August 9th 2007. The FCCs were produced through the merging of bands 2, 3 and 4 of the ETM+ and TM data respectively. The study area was then divided into 32 segments in order to help guide the visual comparison of the two FCC images. Areas which had experienced apparent change in LULC between the May 18th 2003 and August 9th 2007 were subsequently deleted from the vector layer representing LULC for the study area. Furthermore, these deleted areas would be excluded from all LST and NDVI measurements.

In total, 109 LULC polygons were deleted from the LULC layer. Deleted areas represented about 1.8 km^2 or 2.9% of the study area. Most of the areas which had undergone evident change in LULC were in the northern and eastern parts of the study area. These are both areas of Seville which have experienced significant industrial growth in recent times (Sevilla Global, 2010), which might explain the concentration of LULC change within these regions. In Table 2 statistics regarding the deleted LULC polygons are provided.

Table 2. *Statistics of deleted LULC polygons.*

LULC type	**Area (m^2)**	**% of deleted area**
Discontinuous medium density urban fabric	3,283.7	0.2
Sports and leisure facilities	35,605.8	1.9
Discontinuous dense urban fabric	51,469.4	2.8
Continuous urban fabric	177,599.6	9.6
Construction sites	493,790.4	26.7
Industrial, commercial, public, military and private units	1,089,258.7	58.8

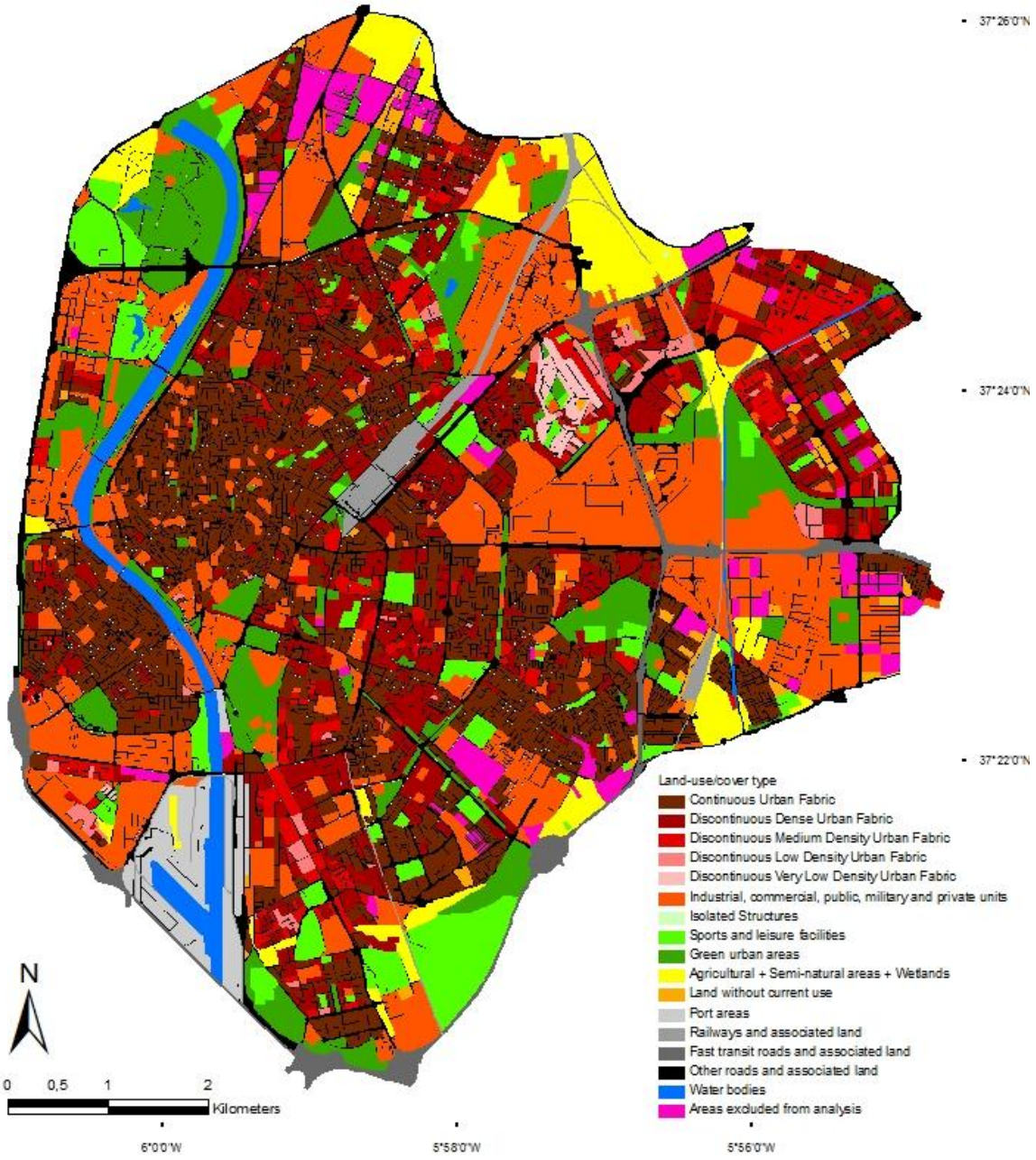

Figure 11. *Spatial pattern of LULC within the study area.*

Figure 11 shows the spatial distribution of LULC types within the study area. Note that polygons that were excluded from LST and NDVI measurements are depicted in bright pink. The size of the study area was approximately 61.9 km^2 (excluding deleted polygons). In Appendix II statistics regarding LULC within the study area are provided, together with a description of each LULC type.

3.3 Data processing

3.3.1 Derivation of NDVI

The red (0.63-0.69 μm) and near-infrared (0.75-0.90 μm) bands (bands 3 and 4 respectively), (NASA, 2010) of the Landsat ETM+ image acquired on May 18th 2003 were used to calculate NDVI values for the study area using the methodology outlined in Sections 3.3.1.1- 3.3.1.3.

3.3.1.1 Conversion of the digital number to spectral radiance

The first step when calculating NDVI from Landsat ETM+ data is to convert the Digital Numbers (DN) of bands 3 and 4 to spectral radiance using the following equation (Landsat Project Science Office, 2001):

$$L_\lambda = ((LMAX_\lambda - LMIN_\lambda)/ (QCALMAX-QCALMIN)) * (QCAL-QCALMIN) + LMIN_\lambda \quad (1)$$

Where: L_λ is the spectral radiance at the sensor's aperture in $Wm^{-2}sr^{-1}\mu m^{-1}$; $LMIN_\lambda$ is the spectral radiance that is scaled to QCALMIN (-5.0 $Wm^{-2}sr^{-1}\mu m^{-1}$ for band 3 and -5.1 $Wm^{-2}sr^{-1}\mu m^{-1}$ for band 4); $LMAX_\lambda$ is the spectral radiance that is scaled to QCALMAX (234.4 $Wm^{-2}sr^{-1}\mu m^{-1}$ for band 3 and 241.1 $Wm^{-2}sr^{-1}\mu m^{-1}$ for band 4); QCAL is the DN; QCALMIN is the minimum quantized calibrated pixel value (corresponding to $LMIN_\lambda$) in DN (0); and QCALMAX is the maximum quantized calibrated pixel value (corresponding to $LMAX_\lambda$) in DN (255).

The values in Equation (1) were supplied by the Landsat Project Science Office (2001), with reference made to the metadata which accompanied the ETM+ image.

3.3.1.2 Conversion of spectral radiance to planetary reflectance

Spectral radiance values for band 3 and 4 were then transformed to planetary reflectance using the following formula (Landsat Project Science Office, 2001):

$$\rho_p = \pi L_\lambda d^2 / (ESUN_\lambda \cos\theta) \quad (2)$$

Where: ρ_p is planetary reflectance; L_λ is the spectral radiance at the sensor's aperture in $Wm^{-2}sr^{-1}\mu m^{-1}$; d is the Earth–Sun distance in astronomical units (1.01142863021849); $ESUN_\lambda$ is the mean solar exoatmospheric irradiance (1533 for band 3 and 1039 for band 4); θ is the solar zenith angle in degrees.

The Earth-Sun distance in astronomical units was retrieved through NASA's HORIZONS Web-Interface (NASA JPL, 2010), while all other values were supplied by the Landsat Project Science Office (2001).

3.3.1.3 Calculation of NDVI

The NDVI was finally calculated using the reflectance values from the red (ρ_{red}) and near-infrared (ρ_{nir}) channels (Tam et al., 2010).

$$NDVI = (\rho_{nir} - \rho_{red})/ (\rho_{nir} + \rho_{red}) \quad (3)$$

3.3.2 Derivation of LST

The thermal band (10.4-12.5 μm) of the Landsat ETM+ sensor was used to derive LSTs over the study area (NASA, 2010). For the Landsat ETM+ sensor, images in the thermal band are captured twice: once in the low-gain mode (band 6L) and once in the high-gain mode (band 6H). Band 6L is used to image surfaces with high brightness, whereas band 6H is used to image surfaces with low brightness (Ma et al., 2010). As the image acquired on May 18th 2003 had relatively low brightness, Band 6H was used in this study.

3.3.2.1 Conversion of the digital number to spectral radiance

The DNs of band 6H from the Landsat ETM+ image acquired on May 18th 2003 were first converted to spectral radiance using Equation (1).

Where: L_λ is the spectral radiance at the sensor's aperture in $Wm^{-2}sr^{-1}\mu m^{-1}$; $LMIN_\lambda$ is the spectral radiance that is scaled to QCALMIN (3.2 $Wm^{-2}sr^{-1}\mu m^{-1}$); $LMAX_\lambda$ is the spectral radiance that is scaled to QCALMAX (12.65 $Wm^{-2}sr^{-1}\mu m^{-1}$); QCAL is the DN; QCALMIN is the minimum quantized calibrated pixel value (corresponding to $LMIN_\lambda$) in DN (0); and QCALMAX is the maximum quantized calibrated pixel value (corresponding to $LMAX_\lambda$) in DN (255).

These values were supplied by the Landsat Project Science Office (2001), with reference made to the metadata which accompanied the ETM+ image.

3.3.2.2 Conversion of spectral radiance to radiant surface temperature

Spectral radiance values for band 6H were then converted to radiant surface temperature under an assumption of uniform emissivity using pre-launch calibration constants for the Landsat ETM+ sensor implemented into the following equation (Landsat Project Science Office, 2001):

$$T_B = K2/ (\ln(K1/ L_\lambda + 1)) \quad (4)$$

Where T_B is radiant surface temperature (in Kelvin); K2 is calibration constant 2 (1282.71 K); K1 is calibration constant 1 (666.09 $Wm^{-2}sr^{-1}\mu m^{-1}$); and L_λ is the spectral radiance at sensor in $Wm^{-2}sr^{-1}\mu m^{-1}$.

All pre-launch calibration constants used in Equation (4) were supplied by the Landsat Project Science Office (2001).

As mentioned above, spectral radiance values were converted to radiant surface temperature under an assumption of uniform emissivity, which means that the calculated radiant surface temperatures are referenced to a blackbody. A blackbody can be defined as a surface that absorbs all incident electromagnetic radiant energy and neither reflects nor transmits this energy. Therefore, a blackbody can be considered an ideal radiator. However, for real solids a

fraction of incident radiant energy will be either reflected or transmitted or both, which is why solids are never ideal radiators (Artis and Carnahan, 1982).

3.3.2.3 Emissivity estimation

Since the radiant surface temperatures derived from Equation (4) are referenced to a blackbody, corrections for Land Surface Emissivity (LSE) according to the nature of LULC become necessary. Emissivity is a ratio which compares the spectral radiant emittance of a surface to that of a blackbody at the same temperature (Artis and Carnahan, 1982). LSE is an important parameter when deriving LSTs as the emissivity of a surface will influence the amount of thermal radiation that it emits. LSE is determined by several factors including the chemical composition, roughness and moisture content of a surface. The emissivity of a surface can have values between 0 and 1, however, for most objects spectral emissivity is very close to 1 (Stathopoulou et al., 2007).

As this research focuses on the environmental impact of urban LULC zoning, emissivities were corrected according to the nature of LULC. Mean surface emissivity estimates for each LULC type were derived based on the methodology presented in Stathopoulou et al., (2007). This method obtains surface emissivity values from the NDVI, (computed in Equations (1-3)) considering the three different cases, which are outlined below (Stathopoulou et al., 2007).

A. NDVI < 0.2

Pixels with NDVI values lower than 0.2 are considered as man-made materials or man-made materials with sparse vegetation. Emissivity (ε) values are obtained from the reflectivity values (ρ) in the red channel, which were calculated in Equation (2).

$$\varepsilon = 1 - \rho_{red} \quad (5)$$

B. NDVI > 0.5

Pixels with NDVI values higher than 0.5 are considered as fully vegetated. These pixels are assigned a typical emissivity value of 0.98 for vegetation.

C. $0.2 \leq NDVI \leq 0.5$

Pixels with NDVI values greater than or equal to 0.2 or less than or equal to 0.5 are considered to be a mixture of man-made materials and vegetation. In this case, the emissivity of a surface is expressed as:

$$\varepsilon = \varepsilon_v P_v + \varepsilon_m(1 - P_v) + d\varepsilon \quad (6)$$

Where: ε is emissivity; ε_v is the emissivity of vegetation (a typical value of 0.98 is assumed); ε_m is the emissivity of man-made materials (a typical value of 0.92 is assumed); P_v is the vegetation proportion (see below); and dε is the fraction of emissivity caused by internal reflections/cavity effect (see below).

$$P_v = (NDVI - NDVI_{min})^2 / (NDVI_{max} - NDVI_{min})^2 \quad (7)$$

Where: $NDVI_{min}$ is 0.2, and $NDVI_{max}$ is 0.5.

$$d\varepsilon = (1 - \varepsilon_m)\varepsilon_v F(1 - P_v) \quad (8)$$

Where: *F* is the shape factor regarding the geometrical structure of vegetation (a value of 0.55 is assumed).

Finally, mean emissivity values were computed for each LULC type using the Zonal Statistics function in ESRI's ArcGIS™ software. Results of the zonal analysis are shown in Table 3.

Table 3. *Surface emissivity values by LULC type.*

LULC type	**Emissivity**
Continuous urban fabric	0.83
Industrial, commercial, public, military and private units	0.84
Port areas	0.86
Other roads and associated land	0.87
Discontinuous dense urban fabric	0.87
Railways and associated land	0.88
Sports and leisure facilities	0.88
Fast transit roads and associated land	0.91
Land without current use	0.91
Discontinuous medium density urban fabric	0.92
Water bodies	0.94
Green urban areas	0.95
Discontinuous low density urban fabric	0.95
Agricultural, semi-natural and wetland areas	0.96
Isolated structures	0.97
Discontinuous very low density urban fabric	0.97

3.3.2.4 Conversion of radiant surface temperature to LST

The calculated radiant surface temperatures were subsequently corrected for emissivity using the following equation developed by Artis and Carnahan (1982):

$$LST = T_B / (1 + (\lambda T_B / \rho) \ln\varepsilon \quad (9)$$

Where LST is land surface temperature (in Kelvin); T_B is radiant surface temperature (in Kelvin); λ is the wavelength of emitted radiance (11.5 μm); ρ is $h \times c/\sigma$ (1.438×10^{-2} m K); h is Planck's constant (6.26×10^{-34}J s); c is the velocity of light (2.998×10^{8} m/sec); σ is Stefan Boltzmann's constant (1.38×10^{-23}J K^{-1}); and ε is emissivity.

Finally, the LSTs were converted into Celsius by subtracting 273.15 from the value calculated in Equation (9).

It should be mentioned that in addition to the method developed by Artis and Carnahan (1982), a few other methods have been developed for deriving LST from Landsat imagery. These include the mono-window algorithm (Qin et al., 2001) and the Radiative Transfer

Equation (Sobrino et al., 2004). However, these other methods require additional input parameters (such as atmospheric water vapor content and near-surface air temperature) from ground-based observations captured simultaneously with the satellite passes, which are usually unavailable (Yang and Liu, 2005; Ma et al., 2010; 22, 27). For this reason, the method developed by Artis and Carnahan (1982), which necessitates no additional input parameters, was chosen for this research.

4. Results

4.1 Visual interpretation of LST and NDVI imagery

The spatial distribution of LST and NDVI within the study area is shown in Figure 12a and b. The areas with the lowest vegetation levels were concentrated within the central and eastern portions of the study area and corresponded to the LULC types “industrial, commercial, public, military and private units”, “continuous urban fabric”, and “discontinuous dense urban fabric”. Low NDVI values also appeared over the Guadalquivir River (which runs north to south through the western portion of the study area).

Conversely, high levels of NDVI indicating the presence of green vegetation were observed, primarily over the outer regions of the study area, and corresponded to the LULC types “discontinuous very low density urban fabric”, “green urban areas”, and “agricultural, semi-natural and wetland areas”. Some pockets of high NDVI were also noticeable within the central portion of the study area and corresponded to “green urban areas” and “sports and leisure facilities”.

In general, the visual pattern of LST was opposite to that of NDVI (with the exception of the land cover type “water bodies”). Hot spots indicating SUHIs were noticeable within the central and eastern portions of the study area and corresponded to the LULC types “industrial, commercial, public, military and private units”, “continuous urban fabric”, and “discontinuous dense urban fabric”. Low LST readings were found mostly in the outer regions of the study area and corresponded to “discontinuous very low density urban fabric”, “green urban areas”, and “agricultural, semi-natural and wetland areas” LULC. Pockets of low LSTs could also be observed within the central portion of the study area and corresponded to “green urban areas” and “sports and leisure facilities”. Low LSTs were also observed over the Guadalquivir River. A prominent feature of the LST image was the sharp contrast between high and low LSTs within the eastern part of the study area where the LULC type “industrial, commercial, public, military and private units” registered very high LSTs and the LULC types “discontinuous very low density urban fabric”, “green urban areas”, and “agricultural, semi-natural and wetland areas” registered very low LSTs.

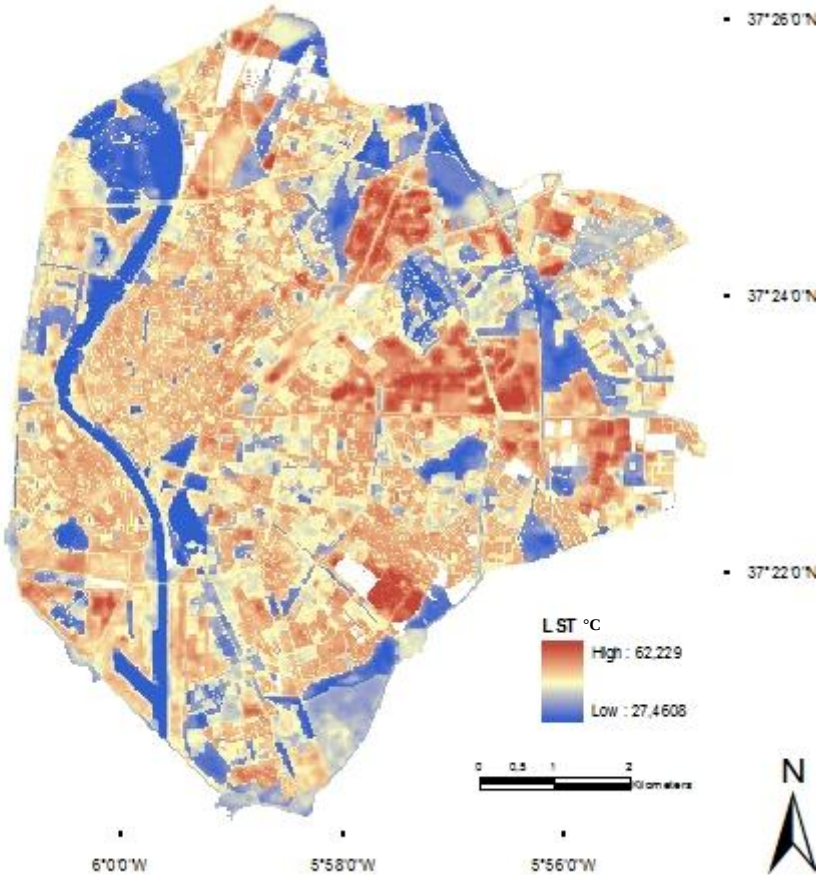

Figure 12a. *Emissivity corrected LST image of the study area (18 May 2003). Computed using the method outlined in Section 3.3.*

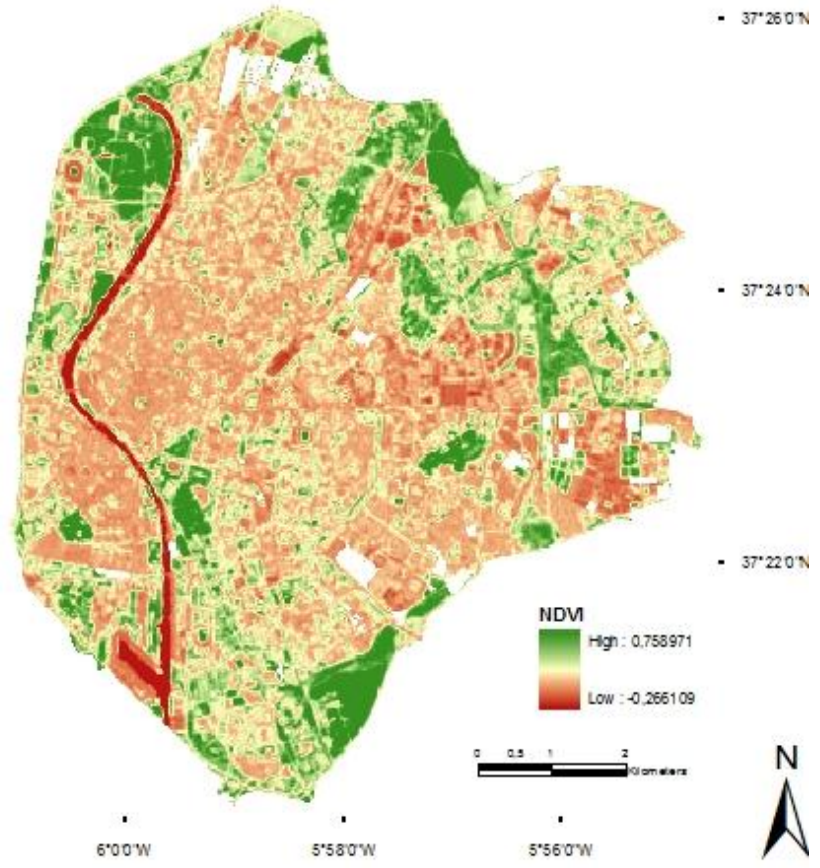

Figure 12b. *NDVI image of the study area (18 May 2003). Computed using the method outlined in Section 3.3.*

4.2 Differences in mean LST and mean NDVI by LULC type

In order to better comprehend the relationship between LST, NDVI, and LULC, the thermal and green space signature of each LULC type was examined. Statistical summaries of LST and NDVI by LULC were derived by means of a zonal summary GIS operation. The results of the GIS zonal statistics are shown in Figure 13a and b. These figures depict mean values of LST and NDVI by LULC type. Numerical statistics of mean LST and mean NDVI values by LULC type are provided in Appendix III.

The LULC type "discontinuous very low density urban fabric" exhibited the highest mean NDVI value (0.385) due to the predominance of vegetated land cover within this LULC type. This was closely followed by the LULC types "agricultural, semi-natural and wetland areas" (0.378) and "green urban areas" (0.36) which also showed high mean NDVI values. These LULC types also exhibited some of the lowest mean LST values for the study area (33.8°C, 36°C, and 35.2°C respectively) which indicates an increased relative rate of evapotranspiration for these LULC types (Wilson et al., 2003).

Following "water bodies", which exhibited a NDVI value of -0.002, the LULC type with the lowest mean NDVI value was "continuous urban fabric" (0.125). The LULC types "industrial, commercial, public, military and public units", "port areas" and "railways and associated land" also showed very low mean NDVI values (0.153, 0.165 and 0.161 respectively). In general, the LULC types with the lowest mean NDVI values exhibited the highest mean LST values. For example, the LULC type "industrial, commercial, public, military and public units" which exhibited the third lowest mean NDVI for the study area (0.153), showed the highest mean LST reading overall (48.5°C). As stated above, the land surface with the lowest mean NDVI reading was "water bodies" due to the lack of vegetation within this LULC type. Since the surface temperature of water rises very slowly (Su et al., 2010), its LST was also lower than all other land surfaces' meaning that the LULC type "water bodies" did not demonstrate an inverse correlation between LST and NDVI, as exhibited by the other LULC types.

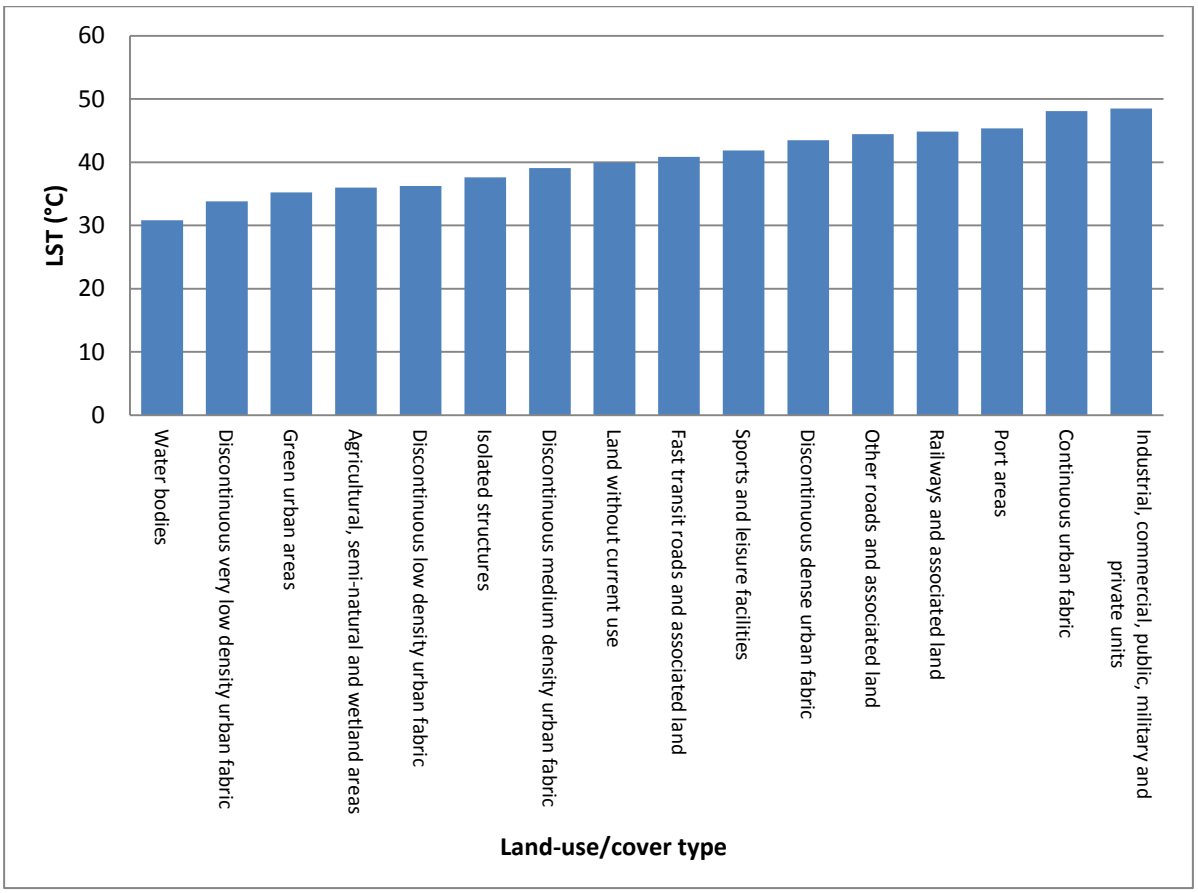

Figure 13a. *Mean values of LST associated with each LULC type.*

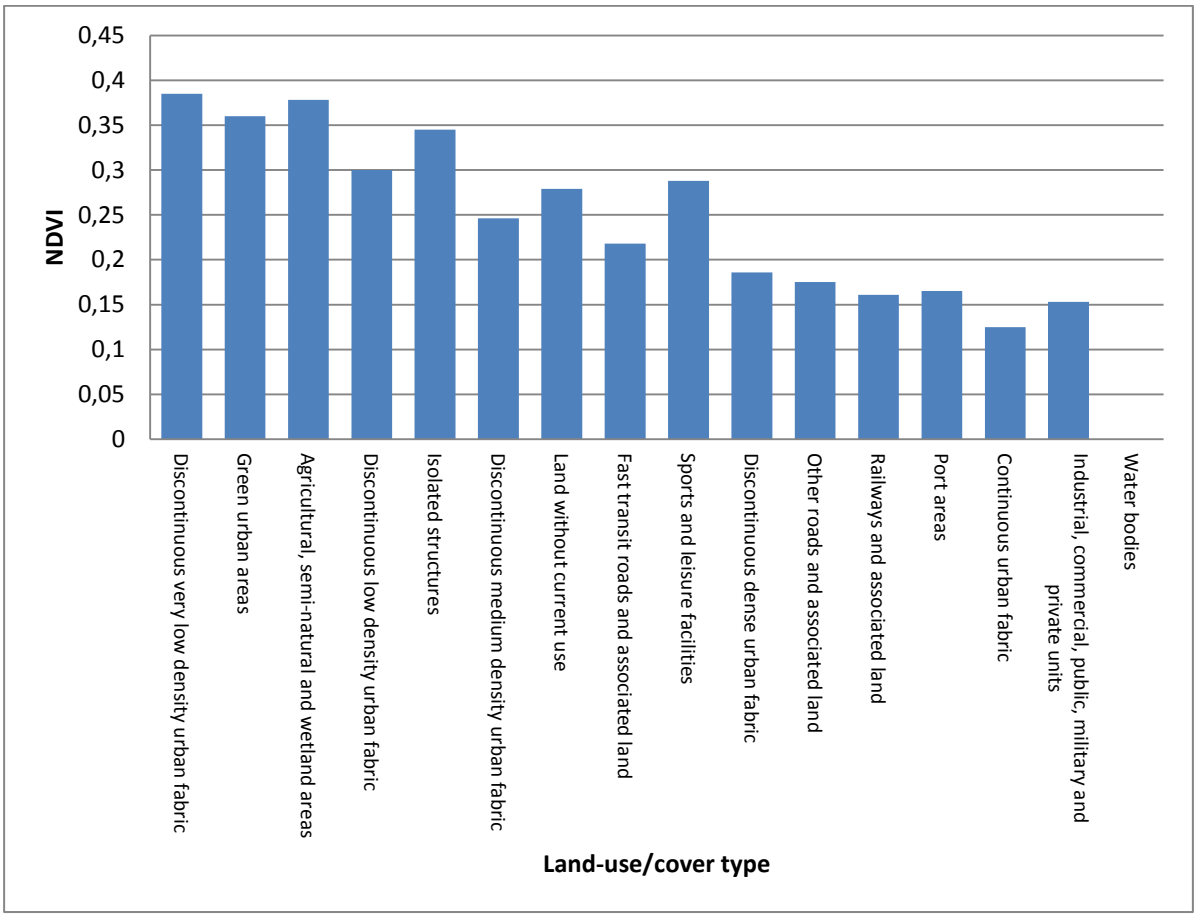

Figure 13b. *Mean values of NDVI associated with each LULC type.*

4.3 Relationship between LST and NDVI

4.3.1 Relationship between LST and NDVI for all LULC polygons

A regression analysis between mean LST and mean NDVI for all LULC polygons (excluding "water bodies") in the study area was conducted. The results of the regression analysis are depicted in Figure 14 where each point represents the mean LST and mean NDVI value associated with one of the 4446 LULC polygons within the study area. As stated above, water features were excluded from the regression analysis. This was done due to the fact that studies have shown that LST and NDVI have a positive correlation with water bodies, meaning that excluding such surfaces would increase the accuracy of the regression between mean LST and mean NDVI values for land surfaces (Yue et al., 2007).

The results indicate a significant inverse correlation between LST and NDVI for the study area. In other words, LULC polygons with high LSTs will generally register low NDVI readings whereas LULC polygons with low LSTs will generally register high NDVI readings.

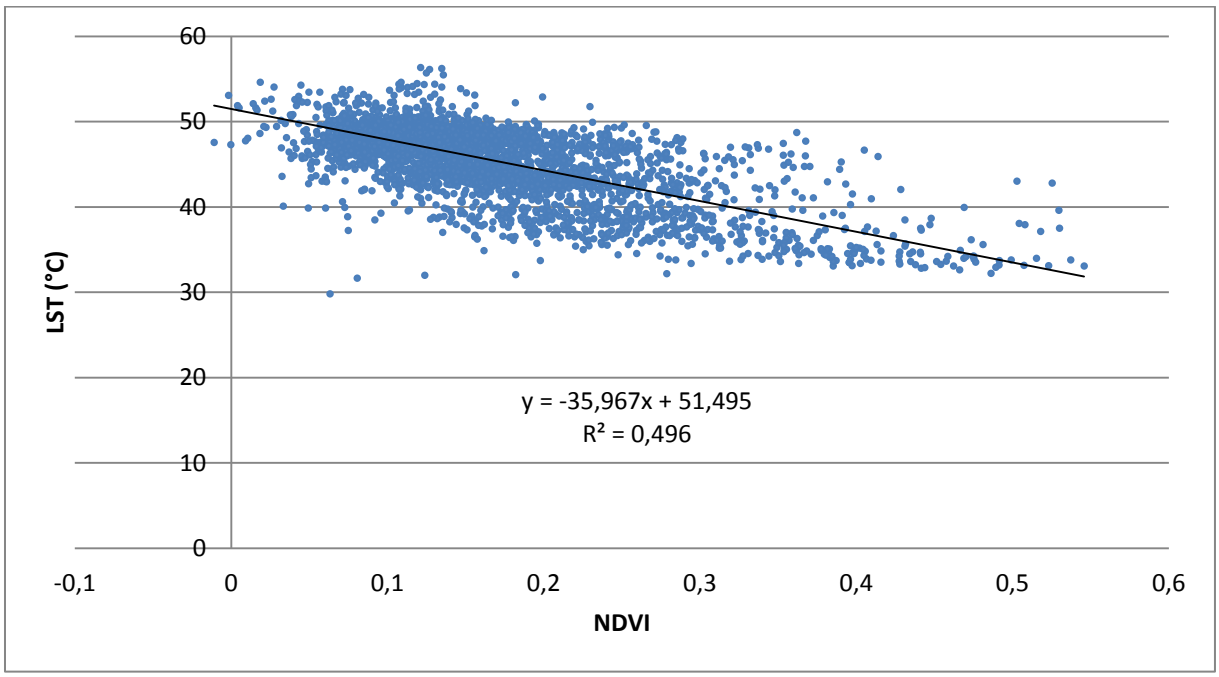

Figure 14. *Linear regression scatter plot of mean LST and mean NDVI associated with every LULC polygon (excluding polygons defined as "water bodies").*

4.3.2 Relationship between LST and NDVI by LULC type

The relationship between LST and NDVI was also quantified for each LULC type, excluding "water bodies". The regression functions between LST and NDVI for each LULC type and coefficient of determination (R^2), which measures the strength of the linear regression, are shown in Table 4. Linear regression scatter plots of mean LST and mean NDVI by LULC type are provided in Appendix IV.

Table 4. *Linear regression results: Mean LST and mean NDVI by LULC type*

LULC type	**Regression function**	**R^2**
Continuous urban fabric	y = -2.1836x + 48.334	0.0046
Discontinuous very low density urban fabric	y = -4.9257x + 35.765	0.1173
Isolated structures	y = -5.1221x + 38.052	1
Port areas	y = -7.0854x + 47.647	0.1072
Discontinuous dense urban fabric	y = -7.0941x + 44.776	0.0881
Sports and leisure facilities	y = -8.0488x + 44.29	0.3148
Other roads and associated land	y = -8.1989x + 46.17	0.1525
Discontinuous medium density urban fabric	y = -8.4135x + 41.096	0.1477
Land without current use	y = -9.1627x + 42.396	0.4461
Green urban areas	y = -9.5703x + 38.988	0.3127
Discontinuous low density urban fabric	y = -11.533x + 39.625	0.3398
Railways and associated land	y = -13.555x + 47.187	0.5172
Agricultural, semi-natural and wetland areas	y = -14.065x + 40.316	0.4381
Industrial, commercial, public, military and private units	y = -15.243x + 50.271	0.2309

Within all LULC types a significant inverse relationship between LST and NDVI was found. The LULC type with the steepest negative regression slope was “industrial, commercial, public, military and private units”, whereas the LULC type which produced the shallowest negative regression slope was “continuous urban fabric”. In other words, with increasing NDVI the LST of “industrial, commercial, public, military and private units” decreases the fastest, while that of “continuous urban fabric” decreases the slowest.

4.3.3 Relationship between LST and NDVI for residential LULC types

In this study, LULC associated with residential use were divided into five different sub-classes based on their degree of soil sealing. These five sub-classes of residential LULC included “continuous urban fabric” (with an average degree of soil sealing >80%), “discontinuous dense urban fabric” (with an average degree of soil sealing >50-80%), “discontinuous medium density urban fabric” (with an average degree of soil sealing >30-50%), “discontinuous low density urban fabric” (with an average degree of soil sealing >10-30%), and “discontinuous very low density urban fabric” (with an average degree of soil sealing <10%) (EEA, 2010b).

As can be observed in Figure 13b, the LULC type with the highest mean NDVI value was “discontinuous very low density urban fabric” (0.385), which is also the residential LULC type with the lowest average degree of soil sealing (EEA, 2010b). As expected, NDVI values for all other residential LULC types decreased with increasing degrees of soil sealing. Thus, the LULC type “continuous urban fabric” which had the highest average degree of soil sealing gave the lowest mean NDVI reading (0.125) amongst the five residential LULC types.

By comparing mean LST and mean NDVI values for the residential LULC types in Figure 13a and b, a general negative correlation between mean LST and mean NDVI values can be

observed. In other words, when comparing all residential sub-classes together, as mean NDVI values decreased with increasing degrees of soil sealing, mean LST values increased.

The linear regression results presented in Table 4 show that the residential LULC type with the highest negative regression slope was "discontinuous low density urban fabric", followed by "discontinuous medium density urban fabric", "discontinuous dense urban fabric", "discontinuous very low density urban fabric", and "continuous urban fabric". This means that the LST of "discontinuous low density urban fabric" is more radically affected by NDVI than the other residential LULC types.

5. Discussion

This study has demonstrated that LULC types and their land surface characteristics are highly related to LSTs and will affect the general pattern of the UHI. Different types of LULC have been shown to vary greatly in their effects on LST and NDVI. Inverse relationships between LST and vegetation abundance were observed for the study area as a whole, and within all LULC types.

As stated above, the LST of "industrial, commercial, public, military and public units" is more radically affected by NDVI than the other LULC types. This implies that a decrease in urban temperatures could be achieved more effectively if vegetation was increased in this LULC type, as it is most conducive to lowering surface temperatures. The fact that the LULC type "industrial, commercial, public, military and public units" was found to be most effective at lowering LST through increased vegetation is encouraging, given that it exhibited the highest mean LST of all LULC types. Moreover, it was apparent through the visual interpretation of the LST and NDVI imagery that this LULC type was responsible for the formation of several hot spots in the study area, indicating SUHIs. Therefore, increasing vegetation abundance within "industrial, commercial, public, military and public units" might prove particularly effective in improving Seville's urban thermal environment.

As the criteria used to determine the density of each of the five residential LULC types was based upon the degree of soil sealing, which is highly related to the percentage of probable vegetation cover, a comparative analysis of the biophysical and thermal characteristics of the various residential LULC types becomes illuminating. The results obtained provided further insight into the manner in which vegetation components of LULC types might impact urban thermal environments as it was found that with increasing degrees of soil sealing (and thus decreasing amounts of vegetation abundance), mean LST values increased.

As mentioned above, Seville has recently been experiencing considerable population growth and it is likely that additional residential areas will be developed in the near future. Moreover, as residential LULC already occupies large portions of the city (nearly 34% of the study area) the thermal characteristics of such LULC will most likely have a considerable impact on Seville's urban thermal environment. For these reasons, analysis into which types of residential LULC are most conducive to decreasing urban surface temperatures through increased vegetation becomes meaningful.

When looking specifically at which residential LULC types are most effective in decreasing surface temperatures through increased vegetation, the results are somewhat disappointing. The urban fabric sub-class "continuous urban fabric" exhibited the second highest mean LST of all LULC types, yet also produced the shallowest regression slope of any LULC type, meaning that with increasing NDVI in this LULC type, LST decreases the slowest as compared to all other LULC types. On the other hand, the residential LULC type "discontinuous medium density urban fabric", which also exhibited a high mean LST, was found to be comparatively much more effective at reducing surface temperatures through increased vegetation.

6. Conclusion

Within the context of climate change and accelerating rates of global urbanization, an understanding of the manner in which urban design strategies might offset consequential negative environmental and social impacts of the UHI becomes imperative. This study focused on the functionality provided by urban vegetation as a means of reducing UHI intensity and moderating the heightened summer temperatures within urban areas which are predicted to occur due to climate change. Recognition and awareness of this functionality is critical as it can serve as a tool for adapting cities to climate change and reducing some of the negative impacts of urban development through improved urban planning and management strategies.

This study found that within the city of Seville, LST and NDVI shared a significant inverse relationship, implying that increasing vegetation abundance will generally reduce surface temperatures and thus UHI intensity. However, this relationship has distinct differences depending on LULC type. Increasing the amount of vegetation in some LULC types will not be as effective at lowering temperatures as in others.

It is hoped that the findings presented in this study may prove useful to those involved in urban and ecological planning in Seville, in terms of illuminating which types of actions may be the most beneficial. For example, this study found that increasing the amount of vegetation within areas defined as "industrial, commercial, public, military and public units" may be particularly effective in reducing urban surface temperatures in Seville, thus reducing the intensity of its UHI. Such knowledge may be particularly useful to those concerned with UHI mitigation, as the city continues to experience considerable growth in industrial activities and the manner in which industrial areas are developed is highly likely to have an impact on the city's thermal environment.

The findings presented in this study related to the types of residential LULC which are most effective at lowering surface temperatures through increased vegetation might also be particularly useful to urban and ecological planning in Seville, as the area is experiencing considerable population growth and future residential expansion will undoubtedly also have an effect on the city's thermal environment. The development of only "discontinuous very low density urban fabric" would, of course, be the most effective due to the low retention of surface temperatures of this LULC type. However, this is often impossible to implement as most urban areas often have too limited an area of available space for this to be practical. However, this study has proven that the LULC type "discontinuous medium density urban fabric", which is a residential LULC type much more common to urban core areas, may be effective at lowering urban temperatures by means of increasing vegetation. Moreover, development of this type of LULC should be elected over "continuous urban fabric" which retains very high surface temperatures and is not as conducive to lowering surface temperatures through increasing vegetation.

The environmental and social consequences of increased temperatures associated with the UHI phenomenon are considerable. These include increased greenhouse gas emissions due to higher energy consumption for air-conditioning, deterioration of air quality, death from heat exhaustion and increased instability of the urban atmosphere. As cities continue to expand, the issue of reducing these types of risks through improved urban planning is of utmost importance, especially in light of predicted climate changes, which may exacerbate the severity of such consequences. Better planning for the preservation and introduction of more urban vegetation may be a simple and effective long-term strategy to confront these challenges.

7. References

AEMET, 2007. Resumen de extremos climatológicos en España. (La Agencia Estatal de Meteorología). Available online at: http://www.aemet.es/documentos/es/divulgacion/resumen_efemerides/Resumen_extremos.pdf (accessed 20 October 2010).

AEMET, 2010. Standard Climate Values – Sevilla. (La Agencia Estatal de Meteorología). Available online at: http://www.aemet.es/es/elclima/datosclimatologicos/valoresclimatologicos?l=5790 (accessed 9 October 2010).

Akbari, H., 2005. Potentials of urban heat island mitigation. International Conference "Passive and Low Energy Cooling for the Built Environment", Santorini, Greece. Available online at: http://www.inive.org/members_area/medias/pdf/Inive%5Cpalenc%5C2005%5CAkbari.pdf (accessed 6 January 2010).

Amiri, R., Weng, Q., Alimohammadi, A., and Alavipanah, S.K., 2009. Spatial-temporal dynamics of land surface temperature in relation to fractional vegetation cover and land use/cover in the Tabriz urban area, Iran. Remote Sensing of Environment, 113, 2606-2617.

Andalucia Com SLU, 2010. Available online at: http://www.andalucia.com/gardens/sevilla/city.htm (accessed 15 October 2010).

Arbor Day Foundation, 2010. Available online at: http://www.arborday.org/takeaction/homedepot2007/ (accessed 8 December 2010).

Artis, D.A., and Carnahan, W.H., 1982. Survey of Emissivity Variability in Thermography of Urban Areas. Remote Sensing of Environment, 12, 313-329.

Arrau, C.P., and Pena, M.A., 2010. The Urban Heat Island (UHI) Effect. Available online at: http://www.urbanheatislands.com (accessed 20 October 2010).

CIMIS, 2009. ET Overview. (California Irrigation Management Information System) Available online at: http://www.cimis.water.ca.gov/cimis/infoEtoOverviewPF.jsp (accessed 14 December 2010).

Climate, 2007. *Köppen classification.* Available online at: http://www.meteorologyclimate.com/koppenclassification.htm (accessed 25 November 2010).

Consorcio de Turismo, 2003. Available online at: http://www.turismo.sevilla.org/paginas_es/portada.asp (accessed 15 October 2010).

EEA, 2010a. GMES Urban Atlas. Available online at: http://www.eea.europa.eu/data-and-maps/data/urban-atlas (accessed 15 September 2010).

EEA, 2010b. Mapping Guide for a European Urban Atlas. Available online at: http://www.eea.europa.eu/data-and-maps/data/urban-atlas Available online at: http://www.eea.europa.eu/data-and-maps/data/urban-atlas (accessed 30 September 2010).

EPA, 2009a. Reducing Urban Heat Islands: Compendium of Strategies – Urban Heat Island Basics. Available online at: http://www.epa.gov/heatisland/resources/pdf/BasicsCompendium.pdf (accessed 22 November 2010).

EPA, 2009b. Heat Island Effect. Available online at: http://www.epa.gov/heatisland/about/index.htm (accessed 22 November 2010).

EPA, 2009c. Reducing Urban Heat Islands: Compendium of Strategies – Trees and Vegetation. Available online at: http://www.epa.gov/heatisland/resources/pdf/TreesandVegCompendium.pdf (accessed 22 November 2010).

Encyclopedia of the Nations, 2010. *Spain.* Available online at: http://www.nationsencyclopedia.com/economies/Europe/Spain.html (accessed 28 November 2010).

FAO, 1998. Crop evapotranspiration - Guidelines for computing crop water requirements - FAO Irrigation and drainage paper 56. Available online at: http://www.fao.org/docrep/x0490e/x0490e00.htm#Contents (accessed 14 December 2010).

Fortuniak, K., 2009. Global environmental change and urban climate in Central European cities. International Conference on Climate Change, The environmental and socio-economic response in the southern Baltic region, Szczecin, Poland. Available online at: http://nargeo.geo.uni.lodz.pl/~meteo/kf/publikacje_kf_PDF/r2009_BALTEX_Szczecin_Fortuniak.pdf (accessed on 10 December 2010).

FSNAU, 2010. Understanding the Normalized Difference Vegetation Index. Available online at: http://www.fsnau.org/downloads/Understanding_the_Normalized_Vegetation_Index_NDVI.pdf (accessed 15 December 2010).

Fuentes, J.M.C., and Rowe, J.G., 1998. The effect of air pollution from nitrogen dioxide (NO_2) on epiphytic lichens in Seville, Spain. Aerobiologia, 14, 241-247.

GADM, 2009. GADM database of Global Administrative Areas. Available online at: http://www.gadm.org (accessed 10 January 2011).

Gay, A.L., and Valverde, J.R., 2010. The comeback of the central city in Southern Europe: population growth and sociodemographic change in the Spanish urban cores. European Population Conference 2010, Vienna, Austria. Available online at: http://epc2010.princeton.edu/download.aspx?submissionId=100918 (accessed 20 November 2010).

Geer, I.W.,1996. Glossary of Weather and Climate, with Related Oceanic and Hydrolic Terms. American Meteorological Society.

Gill, S.E., Handley, J.F., Ennos, A.R., and Pauleit, S., 2007. Adapting Cities for Climate Change: The Role of the Green Infrastructure. Built Environment, 33, 115-113.

Huang, C., Chen, Q., Ying, S., Zhao, F., Shao, Y., Yu, W., Chen, J., Liu, F., Xin, X., and Li, J., 2009. An Analysis on the Coupling Relationship between Urban Vegetation and Land Surface Temperature in Hangzhou based on ASTER Imagery. International Geoscience and Remote Sensing Symposium (2009, Cape Town, South Africa), 3, 338-341.

INE, 2010. Instituto Nacional de Estadistica. Available online at: http://www.ine.es (accessed 16 October 2010).

Kalkstein, L.S., 1991. A New Approach to Evaluate the Impact of Climate on Human Mortality. Environmental Health Perspectives, 96, 145-150.

Kalkstein, L.S., and Smoyer, K.E., 1993. The impact of climate change on human health: some international implications. Experientia, 49, 969-979.

Landsat Project Science Office, 2001. Landsat 7 Science Data User's Handbook (Goddard Space Flight Center). Available online at: http://Landsathandbook.gsfc.nasa.gov/handbook/handbook_htmls/chapter11/chapter11.html (accessed 15 September 2010).

Liao, L., Zhang, L., and Bengtsson, L., 2005. Analyzing Dynamic Change of Vegetation Cover of Desert Oasis Based on Remote Sensing Data in Hexi Region. In: Guodong, C., Zhidong, L., and Bengtsson, L., eds., *Proceedings of the International Symposium on Sustainable Water Resources Management and Oasis-hydrosphere-desert Interaction in Arid Regions.* 279-295.

Lo, C.P, Quattrochi, D.A., and Luvall, J.C., 1997. Application of high-resolution thermal infrared remote sensing and GIS to assess the urban heat island effect. International Journal of Remote Sensing, 18, 287-304.

Ma, Y., Kuang, Y., and Ningsheng, H., 2010. Coupling urbanization analysis for studying urban thermal environment and its interplay with biophysical parameters based on TM/ETM+ imagery. International Journal of Applied Earth Observation and Geoinformation, 12, 110-118.

McPherson, G., Simpson, J.R., Peper, P.J., Maco, S.E., and Xiao, Q., 2005. Municipal Forest Benefits and Costs in Five US Cities. Journal of Forestry, 103, 411- 416.

NASA, 2010. The Enhanced Thematic Mapper Plus. Available online at: http://Landsat.gsfc.nasa.gov/about/etm+.html (accessed 15 December 2010).

NASA JPL, 2010. HORIZONS Web-Interface. (California Institute of Technology) Available online at: http://ssd.jpl.nasa.gov/horizons.cgi (accessed 30 September 2010).

Nichol, J.E., 1994. A GIS-Based Approach to Microclimate Monitoring in Singapore's High-Rise Housing Estates. Photogrammetric Engineering and Remote Sensing, 60, 1225-1232.

NOAA, 2010. Remote Sensing for Coastal Management. Available online at: http://www.csc.noaa.gov/crs/rs_apps/sensors/Landsat.htm (accessed 16 December 2010).

Oke, T.R., 1997. The Nature of Global Environmental Change. Applied Climatology, 1, 273-287.

Parry, M.L., Canziani, O.F., Palutikof, J.P., van der Linden, P.J., and Hanson, C.E., 2007. *Contribution of Working Group II to the Fourth Assessment Report of the Intergovernmental Panel on Climate Change.* (Cambridge University Press). Available online at: http://www.ipcc.ch/publications_and_data/ar4/wg2/en/ch19s19-3-6.html (accessed on 8 December 2010).

Qin, Z., Karnieli, A., and Berliner, P., 2001. A mono-window algorithm for retrieving land surface temperature from Landsat M data and its application to the Israel-Eqypt border region. International Journal of Remote Sensing, 22, 3719-3746.

Ramachandra, T.V., and Kumar, U., 2010. Greater Bangalore: Emerging Urban Heat Island. GIS Development, 14. Available online at: http://www.gisdevelopment.net/application/urban/sprawl/Greater-Bangalore-Emerging-Urban-Heat-Island.htm (accessed 5 December 2010).

Rose, L.A., and Devadas, M.D., 2009. Analysis of and Surface Temperature and Land Use/ Land Cover Types Using Remote Sensing Imagery – A Case in Chennai City, India. Seventh International Conference on Urban Climate, Yokohama, Japan.

Roth, M., 2008. Urban Climate Considerations for the Development of Sustainable Cities. In: *Proceedings for Recent Findings on Planning and Designing Sustainable Cities, Singapore, November 2008.* National University of Singapore. Available online at: http://www.sde.nus.edu.sg/csac/data/WII%20Asso%20Prof%20Matthias%20Roth.pdf (accessed 20 January 2010).

Santana, L.M., 2007. Landsat ETM+ image applications to extract information for environmental planning in a Colombian city. International Journal of Remote Sensing, 28, 4225-4242.

SEOS, 2010. Remote Sensing and GIS in Agriculture. Available online at: http://www.seos-project.eu/modules/agriculture/agriculture-c01-s01.html (accessed 14 December 2010).

Sevilla Global, 2010. Agencia de Desarrollo Integral del Ayuntamiento de Sevilla. Available online at: http://www.sevillaglobal.es (accessed 15 November 2010).

Sevilla Weather, 2009. Available online at: http://www.sevillaweather.com/ (accessed 5 November 2010).

Sobrino, J.A., Jimenez-Munoz, J.C., and Paolini, L., 2004. Land surface temperature retrieval from Landsat TM 5. Remote Sensing of Environment, 90, 434-440.

Stathopoulou, M., Cartalis, C., and Andritsos, A., 2005. Assessing the thermal environment of major cities in Greece. International Conference "Passive and Low Energy Cooling for the Built Environment", Santorini, Greece.

Stathopoulou, M., Cartalis, C., and Petrakis, M., 2007. Integrating Corine Land Cover data and Landsat TM for surface emissivity definition: application to the urban area of Athens, Greece. International Journal of Remote Sensing, 28, 3291-3304.

Su, W., Gu, C., and Yang, G., 2010. Assessing the impact of land use/ land cover on urban heat island pattern in Nanjing city, China. Journal of Urban Planning and Development, 136, 365-372.

Tam, K.C., Lim, H.S., MatJafri, M.Z., and Abdullah, K., 2010. Landsat data to evaluate urban expansion and determine land use/land cover change in Penang Island, Malaysia. Environmental Earth Sciences, 60, 1509-1521.

The City Arborist Program, 2001. Available online at: <www ci austin tx us/trees/res_985 htm> (accessed 8 December 2010).

TreeUtrah, 2010 Available online at: http://treeutah.org/site/ (accessed 8 December 2010).

UN, 2007. World Urbanization Prospects: The 2007 Revision Population Database. Available online at: http://esa.un.org/unup/ (accessed 7 November 2010).

University of Manchester, 2007. Build Parks To Climate Proof Our Cities. *ScienceDaily*. Available online at: http://www.sciencedaily.com- /releases/2007/05/070514101534.htm (accessed 15 November 2010).

USGS, 2010a. The Water Cycle: Evapotranspiration. Available online at: http://ga.water.usgs.gov/edu/watercycleevapotranspiration.html (accessed 15 December 2010).

USGS, 2010b. New Earth Explorer. Available online at: http://edcsns17.cr.usgs.gov/NewEarthExplorer/ (accessed 1 September 2010).

Voogt, J. A., 2002. Urban Heat Island. In : Munn, T., ed., *Encyclopedia of Global Environmental Change*, 3, 660-666 (Chichester: Wiley).

Voogt, J.A., 2004. Urban Heat Island: Hotter Cities. Available online at: http://www.actionbioscience.org/environment/voogt.html (accessed 10 October 2010).

Voogt, J.A., and Oke, T.R., 2003. Thermal remote sensing of urban climates. Remote Sensing of Environment, 86, 370-384.

WateReuse Foundation, 2007. Evapotranspiration: What it is and why it's useful. Available online at: http://www.salinitymanagement.org/Salinity%20Management%20Guide/ew/ew_2.html (accessed 15 December 2010).

Weather Underground, 2010. Available online at: http://www.wunderground.com/history/airport/LEZL/2003/5/18/DailyHistory.html?req_city=NA&req_state=NA&req_statename=NA (accessed 10 October 2010).

Weirer, J. and Herring, D., 2010. Measuring Vegetation (NDVI & EVI). (NASA Earth Observatory). Available online at: http://earthobservatory.nasa.gov/Features/MeasuringVegetation/measuring_vegetation_2.php (accessed 7 December 2010).

Weng, Q., Lu, D. and Schubring, J., 2004. Estimation of land surface temperature-vegetation abundance relationship for urban heat island studies. Remote Sensing of Environment, 89, 467-483.

Wilson, J.S., Clay, M., Martin, E., Stuckey, D., and Vedder-Risch, K., 2003. Evaluating environmental influences of zoning in urban ecosystems with remote sensing. Remote Sensing of Environment, 86, 303-321.

WWF, 2010. Natural Resources. (World Wildlife Fund). Available online at: http://wwf.panda.org/about_our_earth/teacher_resources/webfieldtrips/natural_resources/ (accessed 4 December 2010).

Xian, G., and Crane, M., 2006. An analysis of urban thermal characteristics and associated land cover in Tampa Bay and Las Vegas using Landsat satellite data. Remote Sensing of Environment, 104, 147-156.

Yang, H., and Liu, Y., 2005. A satellite remote sensing based assessment of urban heat island in Lanzhou city , northwest China. In: *Proceedings of the ISPRS Joing Symposium URBAN05 and URSO5, Tempe, March 2005.*Available online at: http://www.isprs.org/proceedings/XXXVI/8-W27/ (accessed 15 February 2010).

Yuan, F., and Bauer, M.E., 2007. Comparison of impervious surface area and normalized difference vegetation index as indicators of surface urban heat island effects in Landsat imagery. Remote Sensing of Environment, 106, 375-386.

Yue, W., Xu, J., Tan, W., and Xu, L, 2007. The relationship between land surface temperature and NDVI with remote sensing: application to Shanghai Landsat 7 ETM+ data. International Journal of Remote Sensing, 28, 3205-3226.

Appendix I

GIS workflow

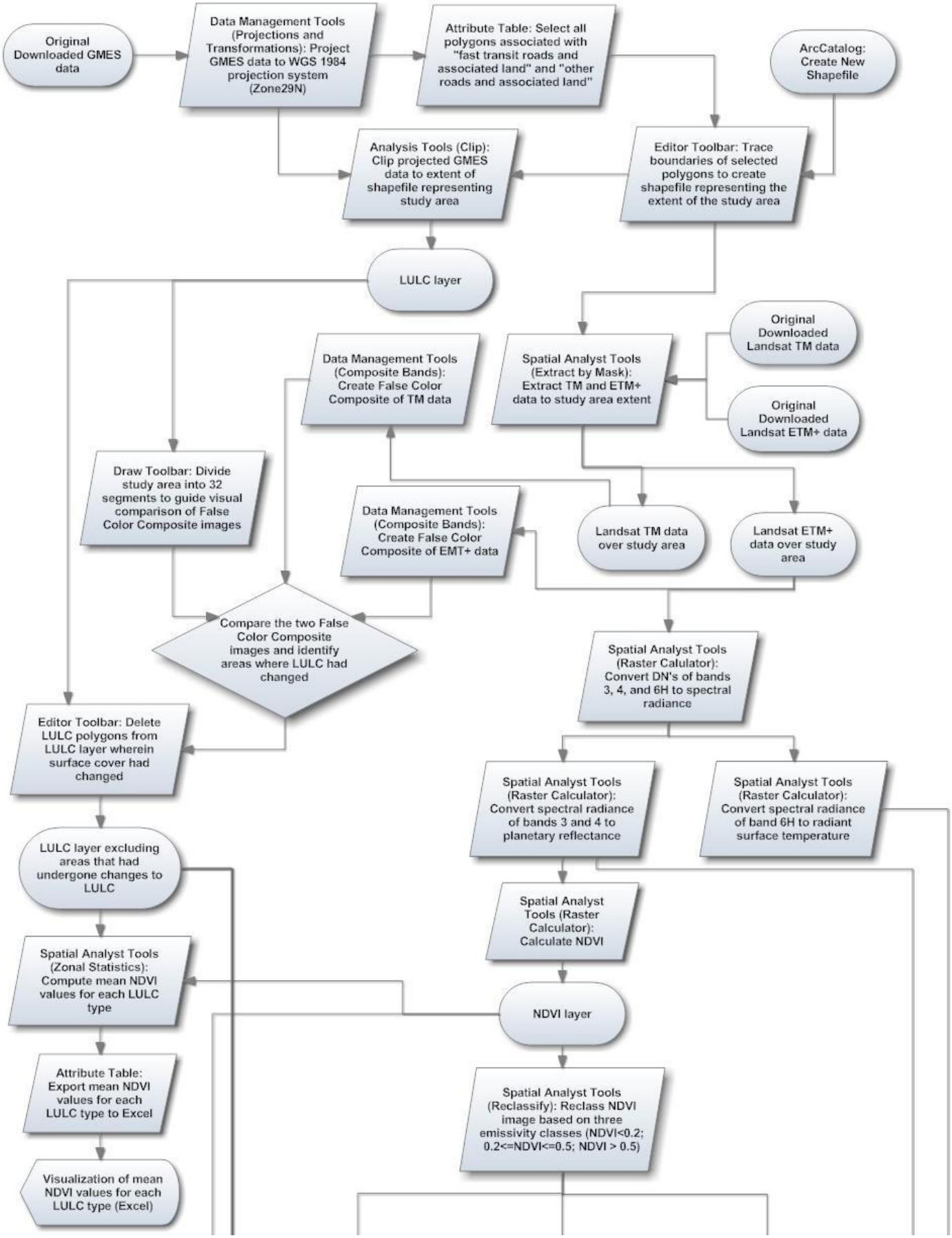

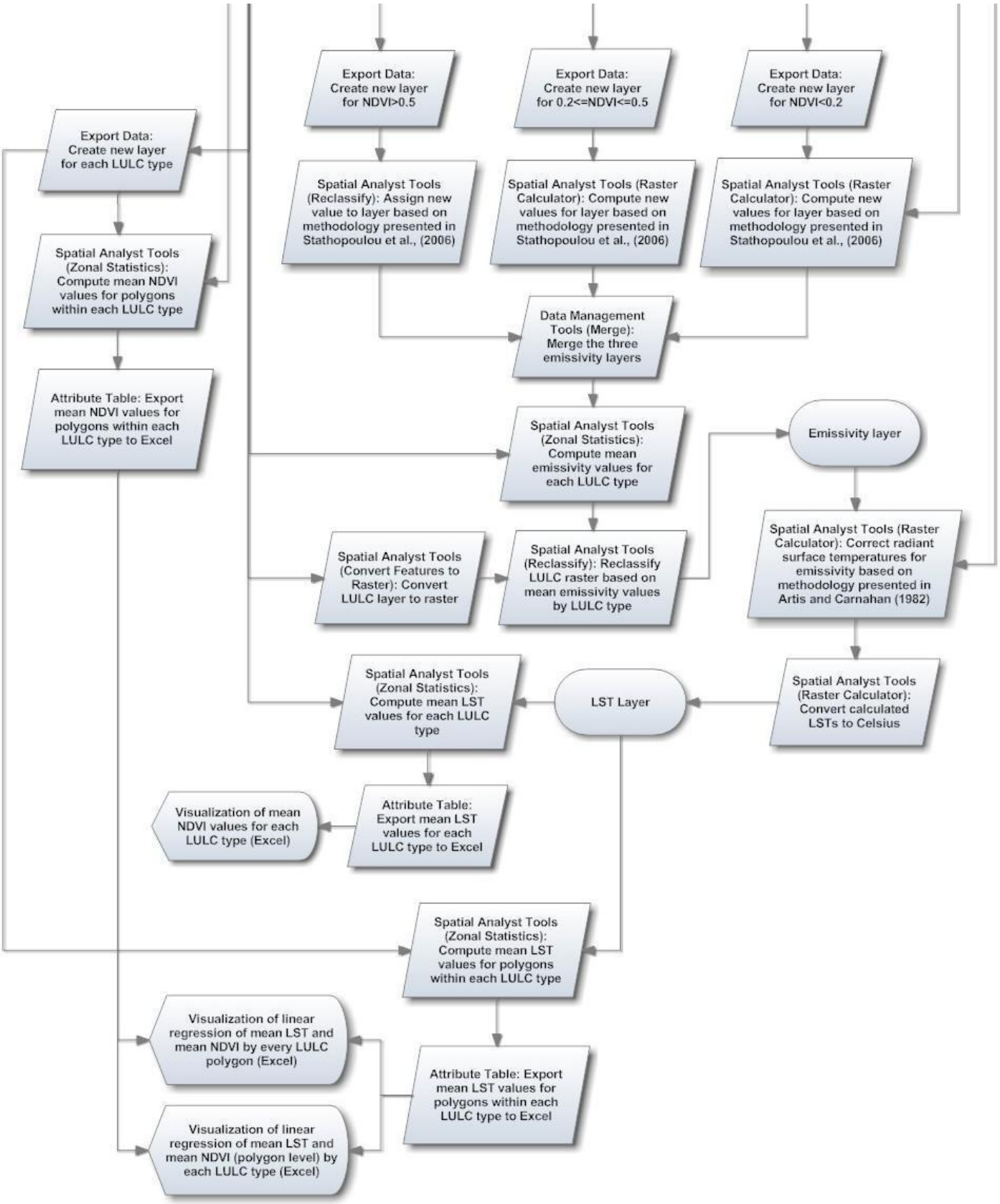
Export Data: Create new layer for NDVI>0.5
Export Data: Create new layer for 0.2<=NDVI<=0.5
Export Data: Create new layer for NDVI<0.2
Export Data: Create new layer for each LULC type
Spatial Analyst Tools (Reclassify): Assign new value to layer based on methodology presented in Stathopoulou et al., (2006)
Spatial Analyst Tools (Raster Calculator): Compute new values for layer based on methodology presented in Stathopoulou et al., (2006)
Spatial Analyst Tools (Raster Calculator): Compute new values for layer based on methodology presented in Stathopoulou et al., (2006)
Spatial Analyst Tools (Zonal Statistics): Compute mean NDVI values for polygons within each LULC type
Data Management Tools (Merge): Merge the three emissivity layers
Attribute Table: Export mean NDVI values for polygons within each LULC type to Excel
Spatial Analyst Tools (Zonal Statistics): Compute mean emissivity values for each LULC type
Emissivity layer
Spatial Analyst Tools (Convert Features to Raster): Convert LULC layer to raster
Spatial Analyst Tools (Reclassify): Reclassify LULC raster based on mean emissivity values by LULC type
Spatial Analyst Tools (Raster Calculator): Correct radiant surface temperatures for emissivity based on methodology presented in Artis and Carnahan (1982)
Spatial Analyst Tools (Zonal Statistics): Compute mean LST values for each LULC type
LST Layer
Spatial Analyst Tools (Raster Calculator): Convert calculated LSTs to Celsius
Visualization of mean NDVI values for each LULC type (Excel)
Attribute Table: Export mean LST values for each LULC type to Excel
Spatial Analyst Tools (Zonal Statistics): Compute mean LST values for polygons within each LULC type
Visualization of linear regression of mean LST and mean NDVI by every LULC polygon (Excel)
Attribute Table: Export mean LST values for polygons within each LULC type to Excel
Visualization of linear regression of mean LST and mean NDVI (polygon level) by each LULC type (Excel)

Appendix II

Table 1. *LULC key for Seville study area. Source: EEA, 2010b.*

LULC type	Description	Number of polygons	% of total study area
Continuous Urban Fabric	Predominant residential use. Buildings and sealed areas cover most of the area. Non-linear areas of vegetation and bare soil are exceptional. Includes downtown areas and central business districts as long there is partial residential use. Average degree of soil sealing: >80%	2,437	18.8
Discontinuous Dense Urban Fabric	Predominant residential use. Non-sealed areas might be common green areas or private gardens. Average degree of soil sealing: >50 - 80%	662	9.8
Discontinuous Medium Density Urban Fabric	Predominant residential use. Non-sealed areas might be common green areas or gardens. Vegetated areas are predominant, however the land is not marked by agriculture or forestry. Average degree of soil sealing: >30 - 50%	197	3.5
Discontinuous Low Density Urban Fabric	Predominant residential use. Non-sealed areas might be common green areas or gardens. Vegetated areas are predominant, however the land is not marked by agriculture or forestry. Average degree of soil sealing: 10 - 30%	69	0.9
Discontinuous Very Low Density Urban Fabric	Predominant residential use. Non-sealed areas might be common green areas or gardens. Vegetated areas are predominant, however the land is not marked by agriculture or forestry. Average degree of soil sealing: <10 %	24	0.5
Isolated Structures	Isolated artificial structures with a residential component, as such as small farm houses.	2	0.01
Industrial, commercial, public, military and private units	Artificial structures with non-residential use (i.e. industrial or commercial uses) or artificial surfaces (e.g. concrete, asphalt), occupy most of the surface. Comprised are also areas with significant amount of green or natural areas but with industrial, commercial, military or public use.	598	21.1
Fast transit roads and associated land	Includes motorways and rest and service areas accessible from motorways.	7	2
Other roads and associated land	Includes roads, crossings, intersections and roundabouts.	36	14.5
Railways and associated land	Railways including railroad stations, cargo stations and service areas.	20	1.4
Port areas	Includes inland harbors and sea ports. Infrastructure of port areas, including dockyards and transport/ storage areas are also included.	28	1.8
Land without current use	Areas in close proximity to artificial surfaces which are waiting to be used or re-used.	58	0.9
Green urban areas	Public green areas such as gardens, zoos and urban parks. Not included are: Private gardens within housing areas, cemeteries, and buildings within parks such as museums.	148	9.1
Sports and leisure facilities	All sports and leisure facilities together with associated land. For example public sport arenas and associated green areas, parking places, etc. Includes golf courses, sports fields, camp grounds and amusement parks.	101	5.3
Agricultural, semi-natural and wetland areas	Includes arable land, permanent crops, pasture and natural grassland, shrubs, herbaceous vegetation, moors and heath land and sparsely vegetated areas.	59	4.7
Water bodies	Includes lakes, fish ponds (natural and artificial), rivers and canals.	22	2.6

Appendix III

Table 1. *Mean LST and NDVI by LULC type.*

LULC type	LST (°C)	NDVI
Water bodies	30.8	-0.002
Discontinuous very low density urban fabric	33.8	0.385
Green urban areas	35.2	0.36
Agricultural, semi-natural and wetland areas	36	0.378
Discontinuous low density urban fabric	36.2	0.3
Isolated structures	37.6	0.345
Discontinuous medium density urban fabric	39.1	0.246
Land without current use	39.9	0.279
Fast transit roads and associated land	40.8	0.218
Sports and leisure facilities	41.9	0.288
Discontinuous dense urban fabric	43.4	0.186
Other roads and associated land	44.4	0.175
Railways and associated land	44.8	0.161
Port areas	45.4	0.165
Continuous urban fabric	48.1	0.125
Industrial, commercial, public, military and private units	48.5	0.153

Appendix IV

Linear regression scatter plots of mean LST and mean NDVI by LULC type

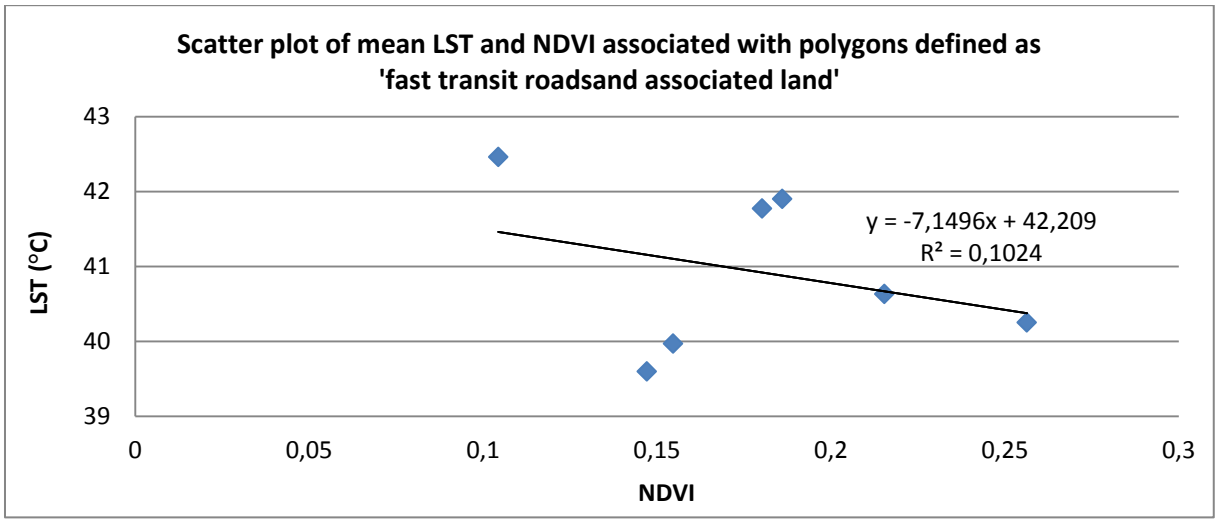

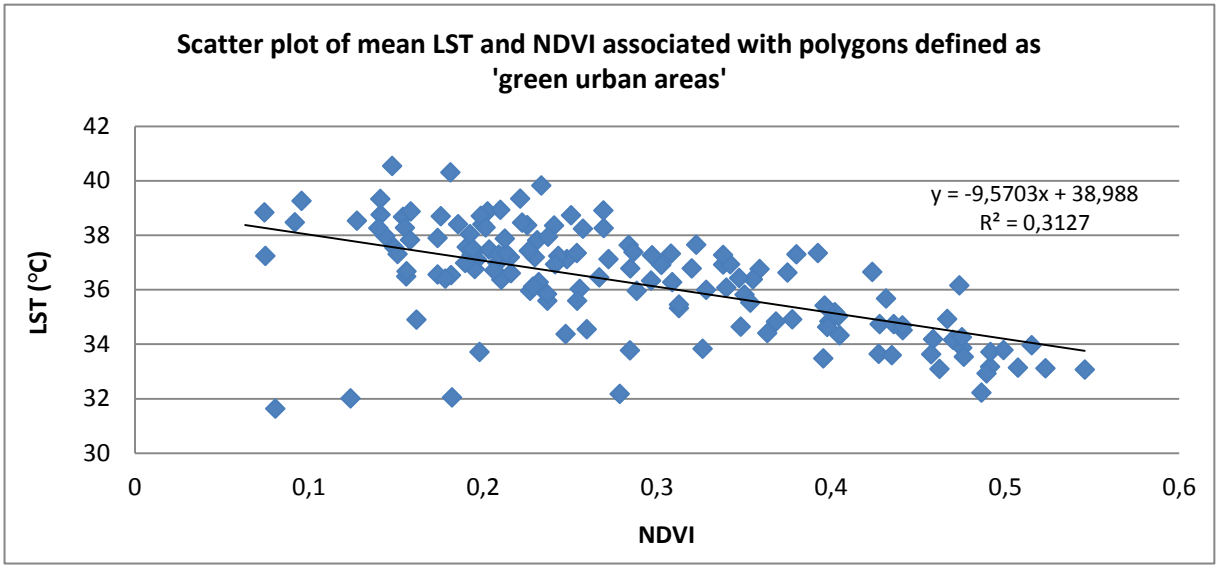

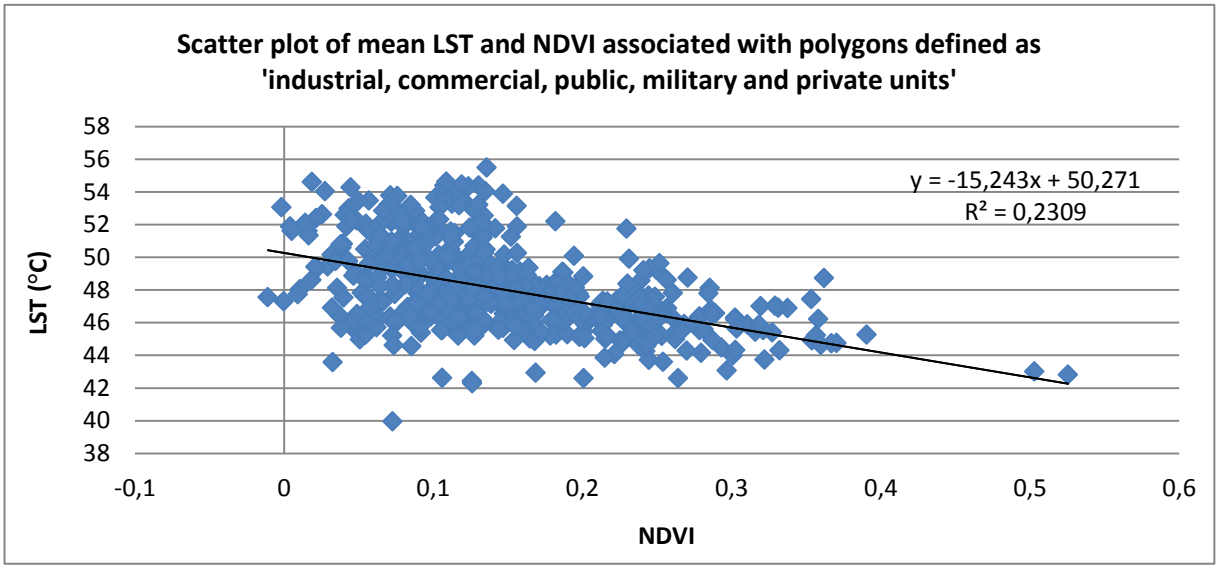

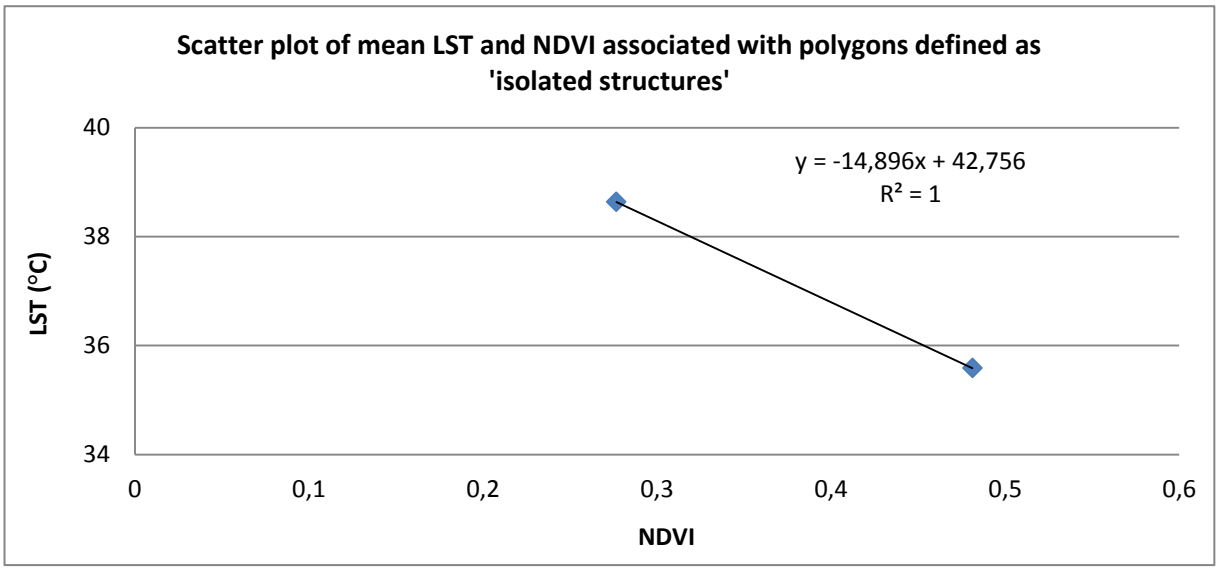
Scatter plot of mean LST and NDVI associated with polygons defined as 'isolated structures'
y = -14,896x + 42,756
R² = 1
LST (°C)
NDVI
40
38
36
34
0
0,1
0,2
0,3
0,4
0,5
0,6

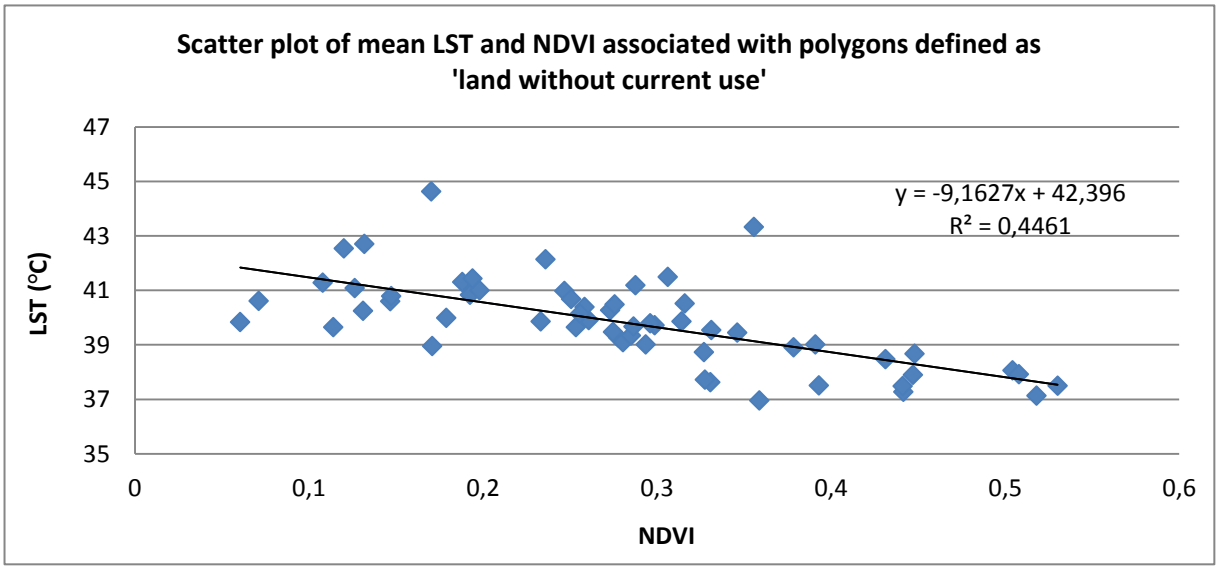
Scatter plot of mean LST and NDVI associated with polygons defined as 'land without current use'
y = -9,1627x + 42,396
R² = 0,4461
LST (°C)
NDVI
47
45
43
41
39
37
35
0
0,1
0,2
0,3
0,4
0,5
0,6

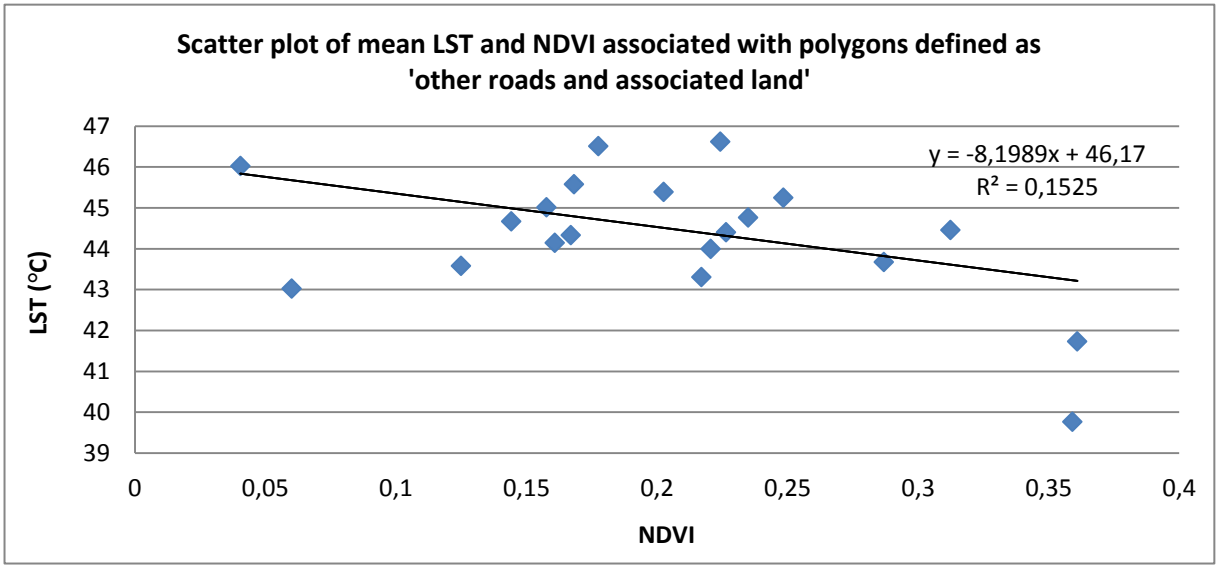
Scatter plot of mean LST and NDVI associated with polygons defined as 'other roads and associated land'
y = -8,1989x + 46,17
R² = 0,1525
LST (°C)
NDVI
47
46
45
44
43
42
41
40
39
0
0,05
0,1
0,15
0,2
0,25
0,3
0,35
0,4

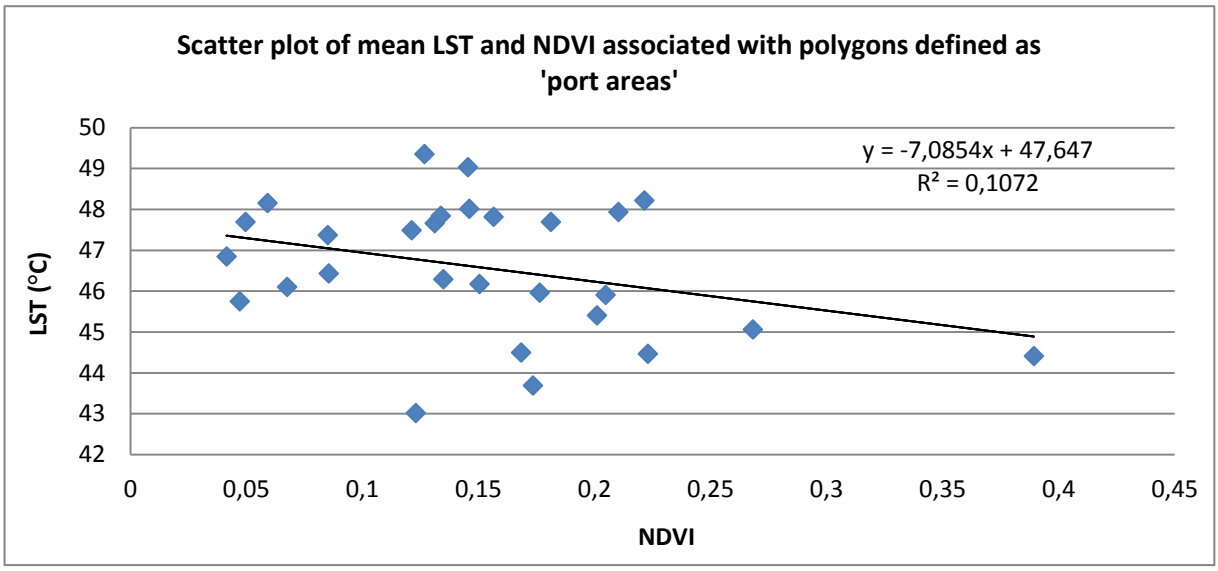
Scatter plot of mean LST and NDVI associated with polygons defined as 'port areas'
y = -7,0854x + 47,647
R² = 0,1072
LST (°C)
NDVI
50
49
48
47
46
45
44
43
42
0
0,05
0,1
0,15
0,2
0,25
0,3
0,35
0,4
0,45

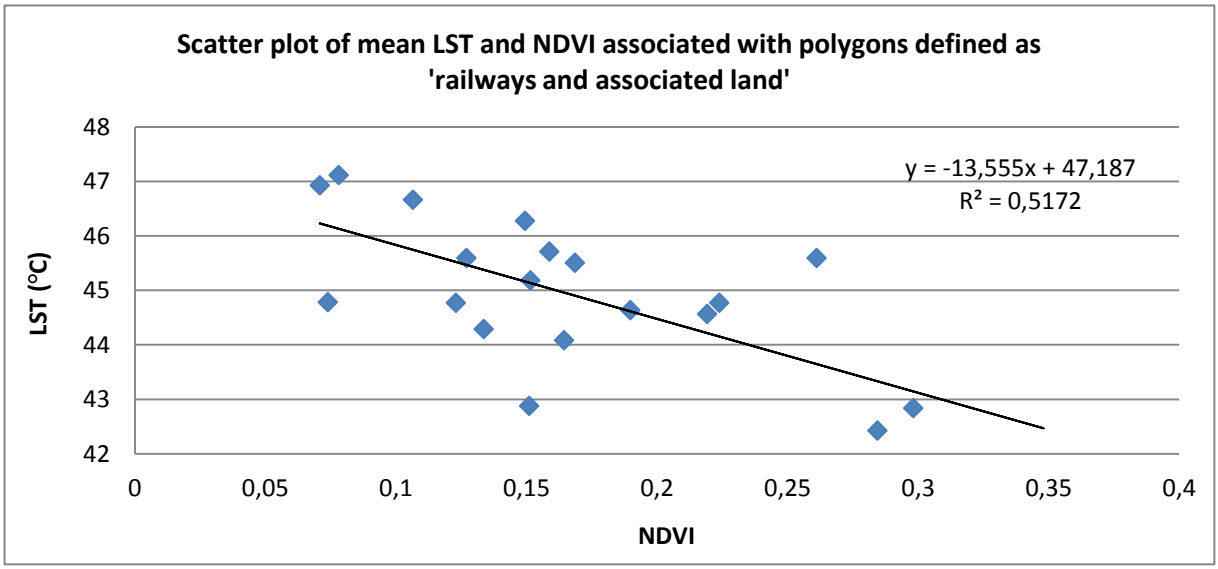
Scatter plot of mean LST and NDVI associated with polygons defined as 'railways and associated land'
y = -13,555x + 47,187
R² = 0,5172
LST (°C)
NDVI
48
47
46
45
44
43
42
0
0,05
0,1
0,15
0,2
0,25
0,3
0,35
0,4

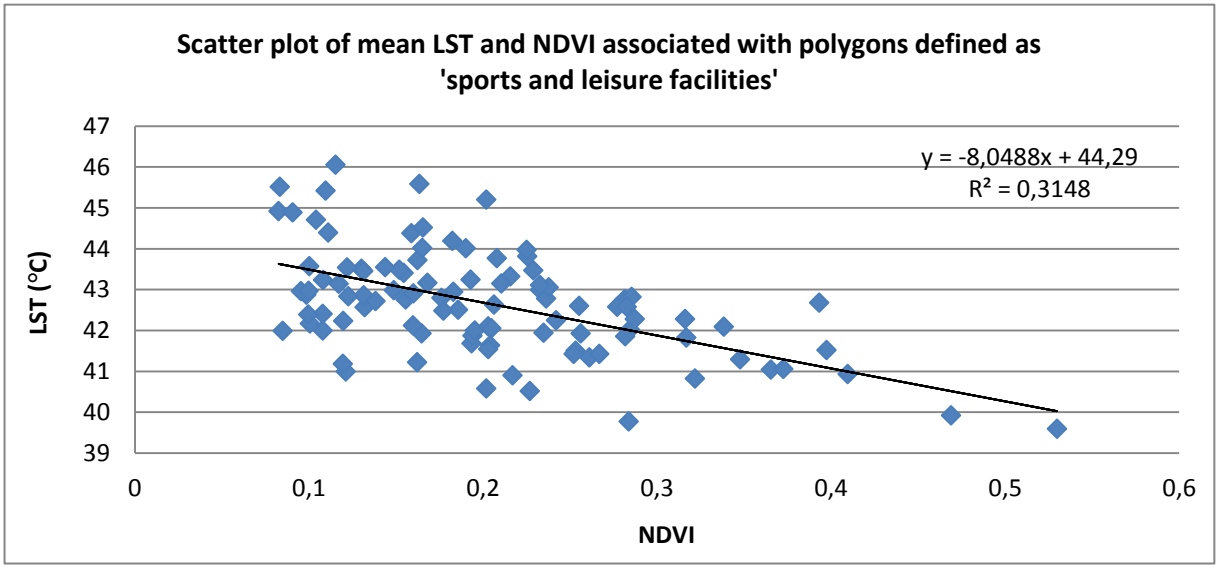
Scatter plot of mean LST and NDVI associated with polygons defined as 'sports and leisure facilities'
y = -8,0488x + 44,29
R² = 0,3148
LST (°C)
NDVI
47
46
45
44
43
42
41
40
39
0
0,1
0,2
0,3
0,4
0,5
0,6

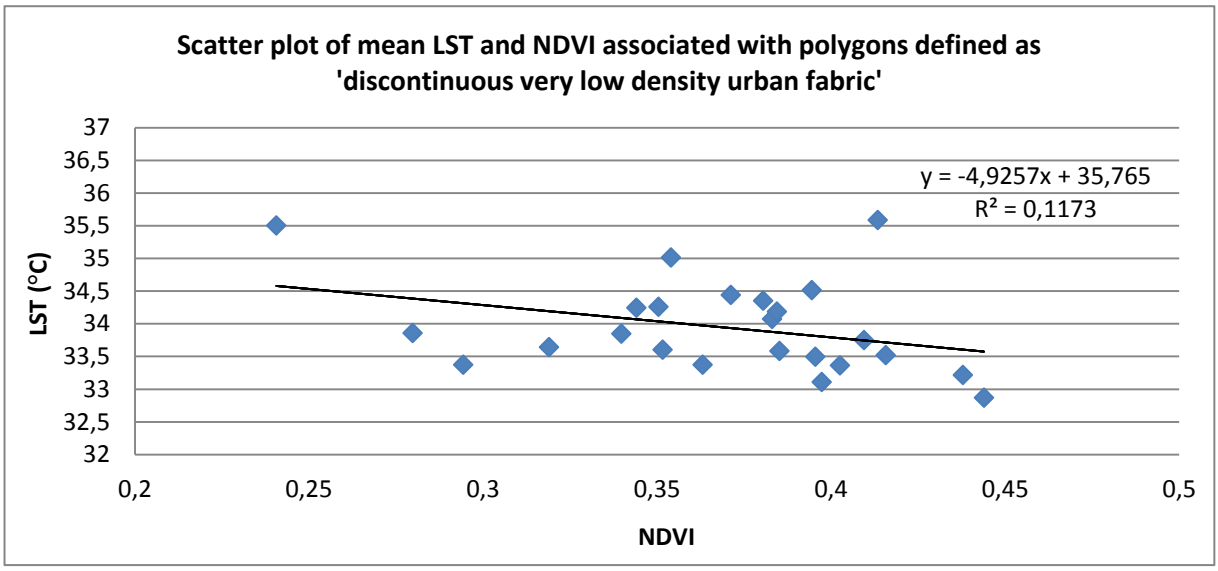
Scatter plot of mean LST and NDVI associated with polygons defined as 'discontinuous very low density urban fabric'
y = -4,9257x + 35,765
R² = 0,1173
LST (°C)
NDVI
37
36,5
36
35,5
35
34,5
34
33,5
33
32,5
32
0,2
0,25
0,3
0,35
0,4
0,45
0,5

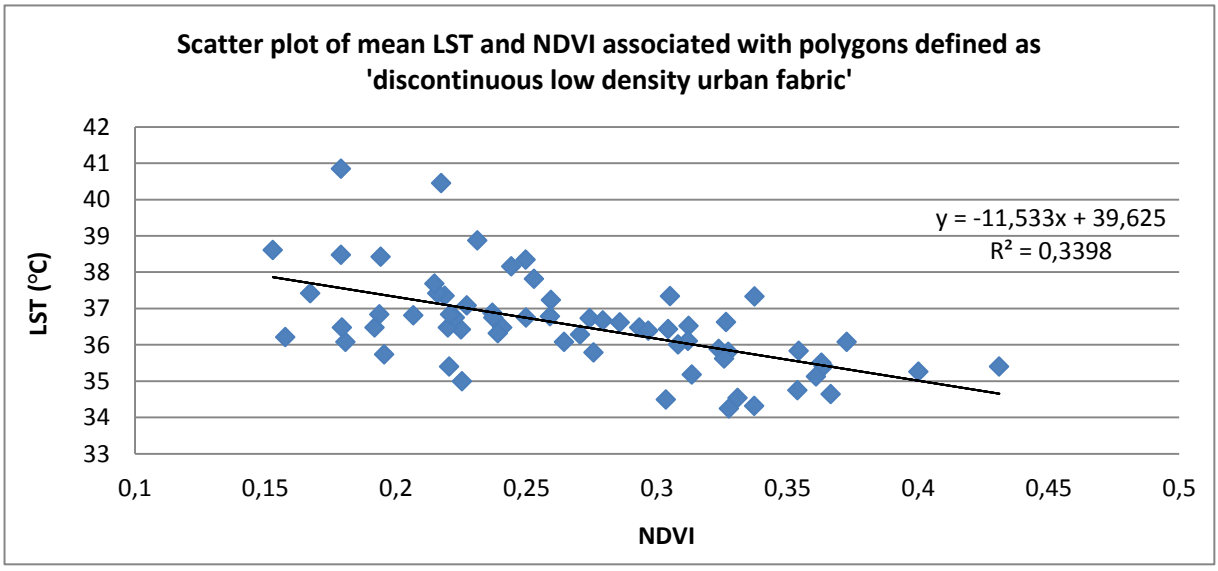
Scatter plot of mean LST and NDVI associated with polygons defined as 'discontinuous low density urban fabric'
y = -11,533x + 39,625
R² = 0,3398
LST (°C)
NDVI
42
41
40
39
38
37
36
35
34
33
0,1
0,15
0,2
0,25
0,3
0,35
0,4
0,45
0,5

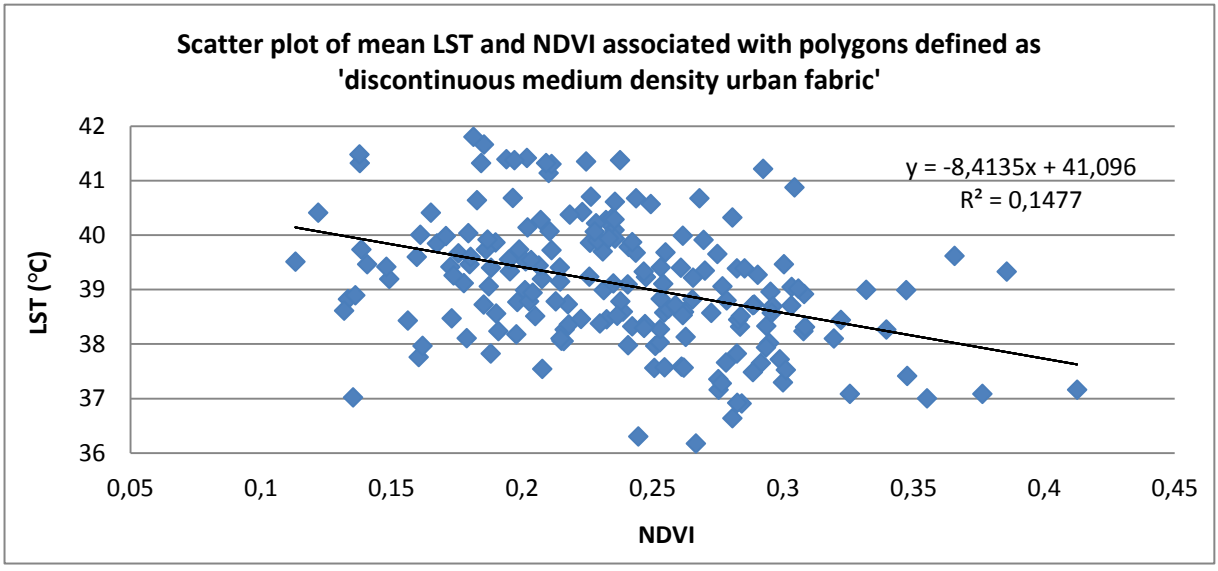
Scatter plot of mean LST and NDVI associated with polygons defined as 'discontinuous medium density urban fabric'
y = -8,4135x + 41,096
R² = 0,1477
LST (°C)
NDVI
42
41
40
39
38
37
36
0,05
0,1
0,15
0,2
0,25
0,3
0,35
0,4
0,45

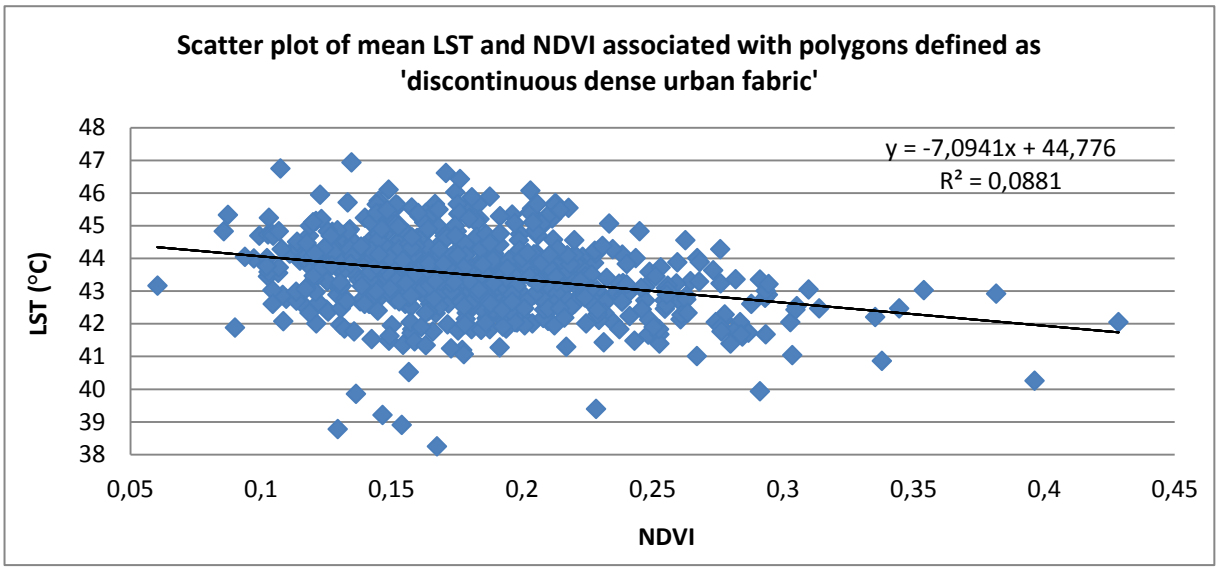
Scatter plot of mean LST and NDVI associated with polygons defined as 'discontinuous dense urban fabric'
y = -7,0941x + 44,776
R² = 0,0881
LST (°C)
NDVI
48
47
46
45
44
43
42
41
40
39
38
0,05
0,1
0,15
0,2
0,25
0,3
0,35
0,4
0,45

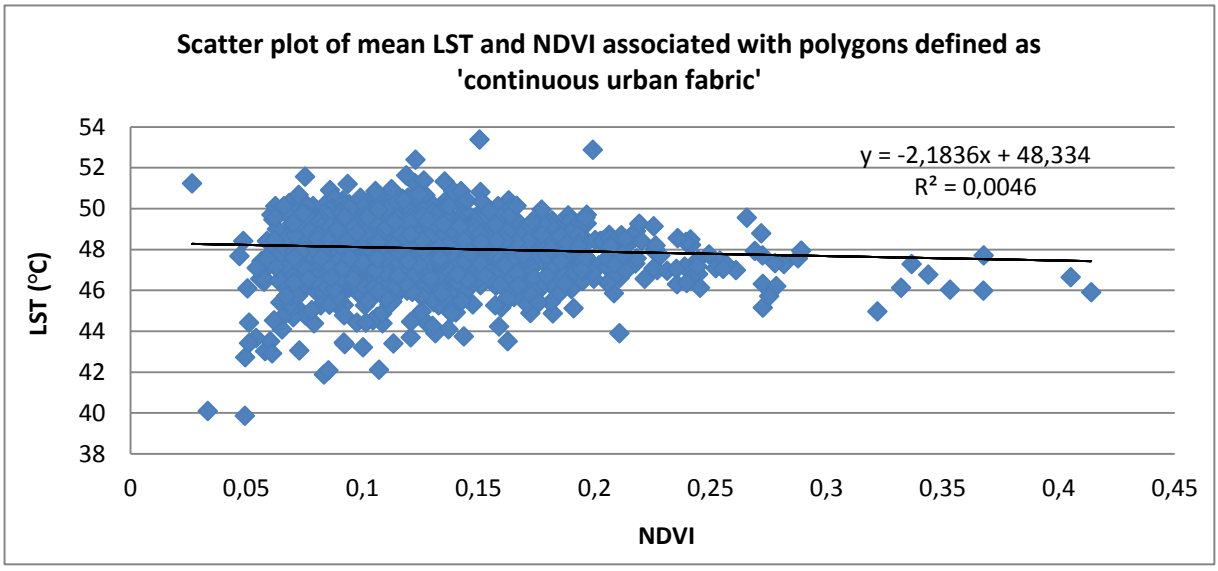
Scatter plot of mean LST and NDVI associated with polygons defined as 'continuous urban fabric'
y = -2,1836x + 48,334
R² = 0,0046
LST (°C)
NDVI
54
52
50
48
46
44
42
40
38
0
0,05
0,1
0,15
0,2
0,25
0,3
0,35
0,4
0,45

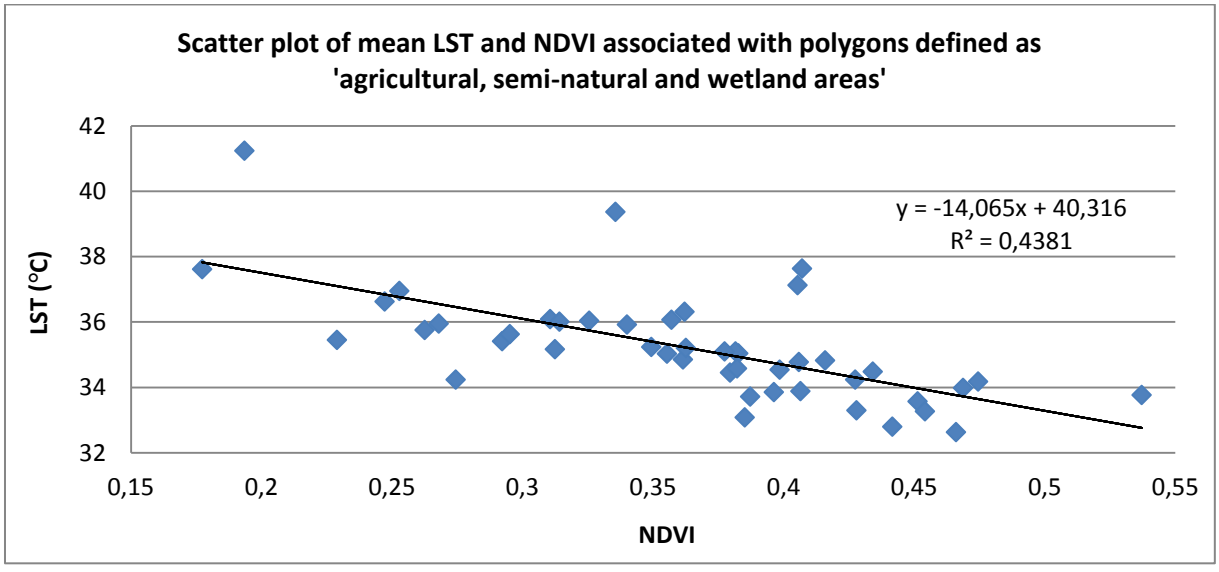
Scatter plot of mean LST and NDVI associated with polygons defined as 'agricultural, semi-natural and wetland areas'
y = -14,065x + 40,316
R² = 0,4381
LST (°C)
NDVI
42
40
38
36
34
32
0,15
0,2
0,25
0,3
0,35
0,4
0,45
0,5
0,55

Appendix V

Table 1. *Spectral and spatial resolution characteristics of Landsat ETM+ bands used in the research. Source: NOAA, 2010.*

Band number	**Spectral resolution (µm)**	**Spatial resolution (m)**
2	0.53 – 0.61	30
3	0.63 - 0.69	30
4	0.78 - 0.90	30
6	10.4 – 12.5	60

Table 2. *Spectral and spatial resolution characteristics of Landsat TM bands used in the research. Source: NOAA, 2010.*

Band number	**Spectral sensitivity (µm)**	**Spatial resolution (m)**
2	0.52 - 60	30
3	0.63 - 0.69	30
4	0.76 - 0.90	30

Series from Lund University's Geographical Department

Master Thesis in Geographical Information Science (LUMA-GIS)

1. *Anthony Lawther:* The application of GIS-based binary logistic regression for slope failure susceptibility mapping in the Western Grampian Mountains, Scotland. (2008).
2. *Rickard Hansen:* Daily mobility in Grenoble Metropolitan Region, France. Applied GIS methods in time geographical research. (2008).
3. *Emil Bayramov:* Environmental monitoring of bio-restoration activities using GIS and Remote Sensing. (2009).
4. *Rafael Villarreal Pacheco:* Applications of Geographic Information Systems as an analytical and visualization tool for mass real estate valuation: a case study of Fontibon District, Bogota, Columbia. (2009).
5. *Siri Oestreich Waage:* a case study of route solving for oversized transport: The use of GIS functionalities in transport of transformers, as part of maintaining a reliable power infrastructure (2010).
6. *Edgar Pimiento:* Shallow landslide susceptibility – Modelling and validation (2010).
7. *Martina Schäfer:* Near real-time mapping of floodwater mosquito breeding sites using aerial photographs (2010)
8. *August Pieter van Waarden-Nagel:* Land use evaluation to assess the outcome of the programme of rehabilitation measures for the river Rhine in the Netherlands (2010)
9. *Samira Muhammad:* Development and implementation of air quality data mart for Ontario, Canada: A case study of air quality in Ontario using OLAP tool. (2010)
10. *Fredros Oketch Okumu*: Using remotely sensed data to explore spatial and temporal relationships between photosynthetic productivity of vegetation and malaria transmission intensities in selected parts of Africa (2011)
11. *Svajunas Plunge:* Advanced decision support methods for solving diffuse water pollution problems (2011)
12. *Jonathan Higgins:* Monitoring urban growth in greater Lagos: A case study using GIS to monitor the urban growth of Lagos 1990 - 2008 and produce future growth prospects for the city (2011).
13. *Mårten Karlberg:* Mobile Map Client API: Design and Implementation for Android (2011).
14. *Jeanette McBride:* Mapping Chicago area urban tree canopy using color infrared imagery (2012)
15. *Andrew Farina:* Exploring the relationship between land surface temperature and vegetation abundance for urban heat island mitigation in Seville, Spain (2012)